ACS Catalysis

Article

Selective hydrogenolysis of glycerol to 1,3-propanediol over rhenium oxide-modified iridium nanoparticles coating rutile titania support

Lujie Liu, Takehiro Asano, Yoshinao Nakagawa, Masazumi Tamura, Kazu Okumura, and Keiichi Tomishige

ACS Catal., **Just Accepted Manuscript** • DOI: 10.1021/acscatal.9b03824 • Publication Date (Web): 21 Oct 2019

is published by the American Chemical Society. 1155 Sixteenth Street N.W., Washington, DC 20036

Selective hydrogenolysis of glycerol to 1,3-propanediol over rhenium oxide-modified iridium nanoparticles coating rutile titania support

Lujie Liu,[a] Takehiro Asano,[a] Yoshinao Nakagawa,[a,b,*] Masazumi Tamura,[a,b]

Kazu Okumura[c] and Keiichi Tomishige[a,b,*]

[a] *Department of Applied Chemistry, School of Engineering, Tohoku University,*

6-6-07 Aoba, Aramaki, Aoba-ku, Sendai, 980-8579, Japan

[b] *Research Center for Rare Metal and Green Innovation, Tohoku University,*

468-1, Aoba, Aramaki, Aoba-ku, Sendai 980-0845, Japan

[c] *Department of Applied Chemistry, Faculty of Engineering, Kogakuin University,*

2665-1 Nakano-machi, Hachioji, Tokyo 192-0015, Japan

* Corresponding authors.

School of Engineering, Tohoku University,

6-6-07, Aoba, Aramaki, Aoba-ku, Sendai, 980-8579, Japan

E-mail: yoshinao@erec.che.tohoku.ac.jp, Tel/Fax: +81-22-795-7215 (Y. N.);

tomi@erec.che.tohoku.ac.jp, Tel/Fax: +81-22-795-7214 (K. T.)

Abstract

The effect of support in Ir-ReO_x catalysts for glycerol hydrogenolysis to 1,3-propanediol was investigated. Rutile TiO_2 support showed high activity, even higher than previously reported SiO_2 support. Anatase TiO_2, C, ZrO_2, CeO_2, Al_2O_3 and MgO supports showed very low activity of supported Ir-ReO_x pairs. Higher Ir-based 1,3-propanediol productivity of Ir-ReO_x/Rutile catalyst was obtained at initial stage even with lower Re/Ir ratio (typical Ir loading amount: 4 wt%, nominal ratio of 0.25; actual ratio of 0.24) without addition of H_2SO_4 than that of Ir-ReO_x/SiO_2. The 1,3-propanediol productivity over Ir-ReO_x catalysts showed dependency on catalyst compositions (metal loading amount), and the relationship between catalyst structure and activity was further established over Ir-ReO_x/Rutile. Relatively high Ir loading amount in comparison with small surface area (6 wt%, on 6 m^2 g^{-1} rutile TiO_2) showed the highest activity (Ir-based activity). Combined characterization results altogether (TPR, TEM, XPS, XAS, CO adsorption, CO FT-IR) with kinetics study, the Ir metal particles interacted with partially oxidized ReO_x cluster (average valence of Re: +3) almost totally covered the surface of rutile TiO_2 particles, and the active site was the Ir-ReO_x interface. Small amount of Ir species (~20%) were incompletely reduced; however such IrO_x species as well as rutile TiO_2 support were not directly involved in glycerol hydrogenolysis. The role of rutile support was regarded as providing unique environment for stabilization of uniform and small Ir-ReO_x particles with very high surface density on rutile TiO_2, which increased the number of active site per Re amount.

Keywords

Iridium, Rhenium, Glycerol hydrogenolysis, 1,3-Propanediol, Rutile titania, Support effect

1. Introduction

Biomass is regarded as an alternative to fossil resources in fine chemicals synthesis, which has been extensively investigated by using heterogeneous catalyst systems in the past decade.[1] Glycerol, as a by-product in manufacturing biodiesel fuel by transesterification of triglycerides to fatty acid esters, is a platform compound for the production of value-added biomass-derived chemicals.[2] Many effective routes, such as dehydration,[2b, 3] oxidation,[4] and selective hydrogenolysis,[5] have been proposed in glycerol chemoselective conversion. The catalytic selective hydrogenolysis of glycerol to 1,3-propanediol (1,3-PrD) has attracted much research interest because 1,3-PrD can be used as a monomer to produce various polymers, including polytrimethylene terephthalate.[2a]

To date, multicomponent-multifunctional noble metal catalysts have been examined for glycerol hydrogenolysis to 1,3-PrD, and Pt-WO_x based[6] and Ir-ReO_x based[5b, 7] catalysts exhibit the most promising performance to obtain high 1,3-PrD yield in water solvent. Glycerol hydrogenolysis over these typical catalysts proceeds under different reaction conditions. Recent reports have shown that higher reaction temperature (413–453 K) at H_2 pressure of 1–8 MPa was required for improving 1,3-PrD production over Pt-WO_x based catalysts,[6a, 6c-e, 8] in contrast to lower reaction temperature (393 K) at typical H_2 pressure of 8 MPa over Ir-ReO_x/SiO_2 catalyst.[7a-c, 9] Although the highest 1,3-PrD yield was obtained with Pt-WO_x based catalyst,[6a] the 1,3-PrD productivity ($P_{1,3\text{-PrD}}$ = (Moles of glycerol × $\text{Yield}_{1,3\text{-PrD}}$ × 76 g mol^{-1}) / (noble metal amount (g) × reaction time (h))) over Pt-WO_x based catalysts was clearly lower than that of SiO_2 supported Ir-ReO_x based catalyst even when they are compared at different temperature optimized for each catalyst (Table S1). In the open literature, the highest 1,3-PrD yield was 66–69% over Pt/WO_x/AlOOH with $P_{1,3\text{-PrD}}$ of 2 g g_{Pt}^{-1} h^{-1},[6a] and the highest $P_{1,3\text{-PrD}}$

obtained among Pt-WO_x based catalysts was 5 g g_{Pt}^{-1} h^{-1} over Pt-WO_x/*t*-ZrO_2 with 49% 1,3-PrD yield (76.2% conversion with 64.8% selectivity to 1,3-PrD at 413 K and 8 MPa for 24 h).[6d] The Ir-ReO_x/SiO_2 catalyst gave the highest 1,3-PrD yield of 38% (81% conversion) over 4 wt%-Ir Ir-ReO_x/SiO_2 (Re/Ir = 0.83, actual ratio) + H_2SO_4 system at 393 K,[7a] whereas the highest $P_{1,3\text{-PrD}}$ was accomplished by high loading amount Ir-ReO_x/SiO_2 (20 wt% Ir, Re/Ir = 0.34, actual molar ratio) catalyst with 22 (initial stage, 23% conversion) and 7 g g_{Ir}^{-1} h^{-1} at highest yield (32%, 69% conversion) without addition of sulfuric acid in our recent work.[9b] In the hydrogenolysis over Ir-ReO_x/SiO_2 catalyst, we have proposed the direct hydrogenolysis mechanism,[7a, 7b, 9b] where Re-OH site binds the terminal OH group of substrate and active hydrogen species with hydride like nature produced at the Ir atoms neighboring to Re species attack the 2-position of the bound substrate. The role of sulfuric acid was serving as stabilizing the adsorption site (Re-O^- + H^+ → Re-OH) and suppressing the leaching of Ir and Re metals[7a-c] or enhancing the interaction between glycerol and Ir-ReO_x/SiO_2 catalyst[5b] rather than altering the reaction pathways. Noble metals are very expensive, and therefore enhancing the activity based on noble metal is of great significance for practical application. Rhenium is also an expensive element,[10] and the usage amount should be also decreased.

One of promising applications of Ir-ReO_x/SiO_2 is selective conversion of a wide range of biomass-derived chemicals.[7a-c, 11] We recently found that severe loss of Re species occurred on some Ir-ReO_x/SiO_2 catalysts during the calcination process for the preparation at high Re loading amount on silica support.[9b] Only about one third of total amount of Re precursor was actually loaded on SiO_2 after calcination (Re: 6.7 wt%, actual amount; 19.4 wt%, assumed amount) over highly active 20 wt%-Ir Ir-ReO_x/SiO_2 (0.34, actual Re/Ir molar ratio; 1, nominal ratio) due to the sublimation of rhenium oxide

at 773 K. Large amount of Re species was wasted, which results in economic issues by the use of expensive Re precursor. Decreasing the calcination temperature definitely increased the actual loading amount of Re on silica support, while the incomplete decomposition of Ir precursor decreased the activity significantly (ca. half).[9b] Another approach is to lower Re loading amount on silica support to suppress the Re_2O_7 sublimation. The 20 wt%-Ir Ir-ReO_x/SiO_2 (Re/Ir = 0.25, nominal) gave almost the same actual ratio as the nominal one.[9b] However, the activity was much decreased by decrease of Re amount, especially for catalyst with lower Ir loading.[7c] To gain insight into the enhanced activity at higher Ir loading amount, the structure of 20 wt%-Ir Ir-ReO_x/SiO_2 (Re/Ir = 0.34, actual) was further clarified. It was suggested that the catalyst structure with ReO_x clusters attached to neighboring Ir nanoparticles facilitated the Ir-ReO_x interface (active site) formation per Re amount.[9b]

The metal–support interaction over supported metal catalysts is a hot topic to reveal how the catalytic performance was influenced by such interaction.[12] The fundamental understanding of support effects refers to stabilizing nanoparticles,[13] promoting electron transfer,[14] encapsulating metal nanoparticles by metal-oxide support[14b, 15] or support directly participating in reaction.[16] Both IrO_2 and RuO_2 have a rutile structure,[17] and the strategy for dispersion of Ir has been employed using rutile as a TiO_2 support.[12b] Smaller particles (1–2 nm) have been observed for Ir and Ir-Au highly dispered on rutile TiO_2 in N_2O decomposition, dehydrogenative synthesis of organics and CO oxidation.[18] On the other hand, in many cases of bimetallic catalysts, the reaction proceeds at the interface of metal–promoter on the support,[19] and the strong metal–promoter interaction can enhance the activity.[20] However, such interaction might be weakened when metal–support and promoter–support interactions become stronger because metal and promoter become individually dispersed on the support. Therefore,

it remains a challenge for development of bimetallic catalysts by the assistance of support properties. In fact, we have developed various bimetallic catalysts for conversion of biomass-related compounds using SiO_2 or C support which are relatively inert supports.[11b-f, 21]

In the present research, the influence of support for Ir-ReO_x catalysts for glycerol hydrogenolysis was investigated in detail, and we found that very high Ir loading amount per surface area of rutile TiO_2 support shows high activity. The required Re amount was relatively low (Re/Ir ≤0.30, actual). The interface of Ir-ReO_x site and how it stabilizes on rutile TiO_2 will be discussed based on activity tests of various related catalysts and characterization results.

2. Experimental Section

Catalysts preparation. Ir-ReO_x/S (S represents support: SiO_2, MgO, CeO_2, γ-Al_2O_3, ZrO_2, activated carbon, H-ZSM-5, anatase TiO_2 (denoted as "Anatase"), rutile TiO_2 (denoted as "Rutile"), and P25 TiO_2 (denoted as "P25") as listed in Table S2) catalysts were prepared by sequential impregnation method according to previous reports:[7a, 7b] Support was firstly impregnated with H_2IrCl_6 aqueous solution. When noted, $Ir(NO_3)_4$ was used instead of H_2IrCl_6. After drying overnight at 383 K, the sample was subsequently impregnated with NH_4ReO_4 solution. Catalyst was eventually obtained after calcined at 773 K for 3 h. Our previous work indicated that calcination at relatively higher temperature was necessary for complete decomposition of H_2IrCl_6 (~773 K), otherwise a significant decline of activity was observed.[9b] In the present work, the calcination temperature was set at 773 K despite the sublimation of rhenium species at this temperature. The loading amount of Ir after the calcination was almost the same considering experimental errors and it is verified that Ir amount is

assumed to be constant during the preparation procedure. Herein, the nominal Re/Ir molar ratio (typically 0.25) was based on the assumed Ir loading amount whereas the actual metal loading amount of both Ir and Re was determined by characterization as described later. The value with a mark (*) of Re/Ir refers to the actual ratio which is calculated by actual Ir and Re amount in this paper while the nominal ratio is shown as "Re/Ir = x, nominal".

Activity test. Glycerol hydrogenolysis was carried out in a stainless steel autoclave (190 ml). Before conducting the reaction, two methods were applied to the reduction of catalyst. One method was the reduction of catalyst in water solvent. Appropriate amount of catalyst and water solvent was introduced to the glass inner vessel, and then it was transferred to the autoclave. The reactor was purged with 1 MPa H_2 for three times to replace the air. Afterwards, the system was heated to 473 K and pressurized to 8 MPa H_2 for reduction treatment for 1 h. Those catalysts that were reduced in the presence of water were called as Ir-ReO_x (L, 473). Then, a certain amount of glycerol was added to the reactor under air at ambient temperature. After removing the air, the system was rapidly increased to reaction temperature (393 K), and then the autoclave was pressurized with H_2 to 8 MPa (defined as 0 h reaction time). We also measured glycerol conversion at 0 h (< 1% conv.) to obtain reliable kinetics results, which was in accordance with our recent work.[9b] The stirring rate was fixed at 500 rpm to eliminate mass transfer effects. The other method refers to the catalysts reduced by H_2 flow (100% H_2, 30 mL min^{-1}) at various temperatures for 1 h using a fixed-bed reactor. These samples after gas-phase reduction were denoted as (G, xxx), similarly to the case of catalysts reduced by liquid-phase reduction (L, xxx). For example, Ir-ReO_x (G, 473) means catalysts reduced by H_2 flow at 473 K for 1 h. All the gas-phase reduced catalysts were introduced to the reactor under N_2 atmosphere to avoid oxidation of

catalyst by the contact with air unless noted; in some cases, catalyst after reduction was passivated by 1 % O_2/He for 15 min to examine the catalyst stability under air. Subsequently, same operation was performed: purging the N_2 with H_2, heating to 393 K, and pressurizing to 8 MPa to start the reaction. For both methods, the standard reaction conditions were the same and described as follows: 4 g (43 mmol) of glycerol, 2 g of water, and 150 mg of 4 wt%-Ir Ir-ReO_x/TiO_2 (6 mg, 31 μmol Ir), 8.0 MPa H_2, reaction temperature at 393 K for 4 h. Some of the parameters were sometimes changed and the details can be found below the table or figure. In regard to reuse test, Ir-ReO_x/Rutile catalyst was firstly reduced in H_2 flow (G, 573) and introduced into the reactor under N_2. After the first run, decantation method was used to easily obtain the wet form catalyst under N_2 atmosphere after reaction due to the hydrophobic property of rutile TiO_2 support.[17b] The inductively-coupled plasma atomic emission spectrometry (ICP-AES, Thermo Fisher iCAP6500) was employed to measure the leached Ir and Re amount in these solutions. In the following runs, no further reduction was performed, and water solvents with and without being degassed were both selected for comparison. The weight of glycerol and water in each run was adjusted to keep at a constant ratio of glycerol/water/catalyst.

Product analysis. The products in the liquid phase were quantified by gas chromatograph (Shimadzu GC-2025) equipped with a TC-WAX capillary column (diameter 0.25 mm, 30 m) using 1-butanol as an internal standard, while the gas phase products were quantified by gas chromatograph with a Rtx-1-PONA capillary column (diameter 0.25 mm, 100 m) using standard gases (methane, ethane and propane) to obtain calibration curve. These products were also identified by GC–MS (QP5050, Shimadzu). The propane (main gas-phase product) and C–C cracking products are defined as “Others” in this work. The conversion and selectivity were determined on the carbon basis as

described in our recent work.[9b] The mass balance was examined and the difference of each result was within the experimental error of ±10%. The productivity of 1,3-PrD ($P_{1,3\text{-PrD}}$) was calculated as previously reported:[9b] $P_{1,3\text{-PrD}}$ = (Moles of glycerol × $\text{Yield}_{1,3\text{-PrD}}$ × 76 g mol^{-1}) / (Ir amount (g) × t (h)). The glycerol conversion rate (v_g) was determined from converted glycerol (mmol) amount per catalyst amount (g) per hour (h).

Catalyst characterization. The surface areas of various supports were obtained on an instrument (Micromeritics Gemini) by N_2 adsorption (BET method). A wavelength dispersive X-ray fluorescence (XRF) instrument (Bruker, S8 Tiger) was used to measure the actual loading amount of iridium and rhenium on TiO_2 support under He atmosphere. The calcined catalyst (0.8 g) and internal standard ZrO_2 (0.1 g) were well mixed prior to measurement, and calibration curve was produced by using commercially available IrO_2 and ReO_2 as previously reported in our recent work.[9b] The amount of Ir and Re over typical samples (4 wt%-Ir, Re/Ir = 0.25 and 1, nominal) after gas-phase reduction or reaction was also examined by XRF, and the values were almost the same to those after calcination. The measurements were repeated three times for typical samples, and the experimental error of actual Re/Ir^* ratio was within ± 0.04. Temperature-programmed reduction (TPR) patterns were obtained with a home-made fixed-bed flow reaction system. The catalyst (~100 mg) in a glass tube was heated under the 5% H_2/Ar (30 mL min^{-1}) at 10 K min^{-1} from 300 to 1000 K. The consumed H_2 amount was calculated based on the signal intensity area of thermal conductivity detector (TCD), which corrected by the consumed H_2 amount of calcined 4 wt% Ir/SiO_2.

The transmission electron microscope (TEM) imaging of samples was performed on HITACHI HF 2000EDX apparatus. The samples after reduction were suspended in ethanol solvent, and dropped

on Cu grids. Average particle size was calculated by $\Sigma n_i d_i^3/\Sigma n_i d_i^2$ (d_i: particle size; n_i: number of particle with size d_i). CO chemisorption measurement employed a volumetric method at ambient temperature by using high-vacuum system. Prior to measurement, catalysts were reduced at 573 K by H_2 flow. The pure CO pressure after adsorption was about 1.1 kPa. The acquired CO adsorption amount was assumed to be equal to that of the surface Ir atoms, which further determined the Ir dispersion by CO/Ir (D_{CO}). FT-IR spectra of adsorbed CO on catalysts were performed in an *in-situ* cell by diffuse reflectance mode on Nicolet 6700 FT-IR. Samples were put into a cup and reduced with H_2 at 573 K in the cell, which corresponds to (G, 573) pre-reduction for the activity test. CO pulses were introduced into the system at ambient temperature using N_2 as a carrier gas until the adsorption reached saturation, and the intensity of each spectrum was normalized by adjusting the relative peak area to corresponding D_{CO}.

X-ray photoelectron spectra (XPS) were obtained on the Shimadzu AXIS-ULTRA DLD spectrometer under high vacuum at ambient temperature. The binding energy was calibrated with C 1s peak of sample-loaded adhesive tape at 284.6 eV. Samples after pre-reduction at 573 K by H_2 flow were directly introduced to the analysis chamber under N_2 atmosphere without exposure to air. For catalyst after passivation, the reduced catalyst was treated with 1% O_2/He for 15 min at ambient temperature, and then loaded into the chamber. The curve fitting of XPS results was performed with the software CasaXPS, ver. 2.3.19 (Casa software Ltd.). In the case of Ir 4f pattern, the two signals for Ir $4f_{7/2}$ and Ir $4f_{5/2}$ were separated by 3.0 eV at a fixed relative peak ratio of 4:3 and full width at half-maximum (fwhm) ratio of 1:1. For Re 4f pattern, the difference of peak separation by 2.4 eV for Re $4f_{7/2}$ and Re $4f_{5/2}$, and the relative peak ratio and peak widths were similarly set as the theoretical values.

The patterns were fitted by Gaussian functions and Lorentzian asymmetric functions for Ir and Re, respectively. In addition, the curve fitting for Ti 2p was also employed at fwhm ratio of 2:1 for Ti $2p_{1/2}$ to Ti $2p_{3/2}$ using Gaussian functions.

The X-ray absorption near edge structure (XANES) and extended X-ray absorption fine structure (EXAFS) spectroscopy was measured with the approval of Japan Synchrotron Radiation Research Institute (JASRI; Proposal No. 2019A1369 and 2019A1716), and details of measurement and analysis are shown in Supporting Information. The sample preparation method was as follows: In the case of catalyst after calcination at 773 K, the powder was directly filled into a plastic bag for measurement. For the reduced catalysts, samples were pre-reduced at 573 K for 1 h by H_2 flow. After cooling, they were transferred to a plastic bag under N_2 atmosphere. The catalyst after reaction (same reaction conditions to the reuse test) was also collected under N_2 atmosphere, dried after washing with methanol, and then placed into a plastic bag. The thickness of all the samples was about 2 mm, which gave the edge jump for Ir L_3-edge at 0.2–0.7 (transmission mode) and Re L_3-edge at 0.001–0.005 (fluorescence mode), respectively.

3. Results and discussion

Optimization of Ir-ReO_x catalysts in hydrogenolysis of glycerol to 1,3-propanediol. The Ir-ReO_x pairs with fixed Ir amount (4 wt%) at a ratio of Re/Ir = 0.25 (nominal) were loaded on various supports, and their activities in glycerol hydrogenolysis were measured (Figure 1A). The reduction temperature was increased from 473 K which was the typical temperature for complete reduction of Ir-ReO_x/SiO_2[7a-c, 9b] to 573 K, since higher temperature is generally necessary to reduce metal oxide species which are more strongly interacted with reducible TiO_2 relative to SiO_2 support.[22] The Ir-

ReO_x/Rutile demonstrated the highest activity with high selectivity to 1,3-PrD in comparison with other screened supports including SiO_2 which has been used in both our works and other researchers' works for Ir-ReO_x-catalyzed hydrogenolysis.[5b, 7a, 7b, 7d, 9b] Interestingly, the performance of TiO_2-supported catalysts much depended on the crystalline phase of TiO_2, and glycerol hydrogenolysis hardly proceeded over Ir-ReO_x/Anatase. Ir-ReO_x catalyst supported on P25 TiO_2 which is a mixture of rutile and anatase showed an activity between those of Ir-ReO_x/Anatase and Ir-ReO_x/Rutile. The activity of Ir-ReO_x/H-ZSM-5 was also higher than that of Ir-ReO_x/SiO_2, although it was lower than that of Ir-ReO_x/Rutile. The good activity of Ir-ReO_x/H-ZSM-5 can be related to the small external surface area of H-ZSM-5 zeolite: Ir particles might be densely located on the external surface of H-ZSM-5 and Re species, similarly to the case of high-loading Ir-ReO_x/SiO_2 catalyst.[9b] Moreover, the acidity of H-ZSM-5 in hot water solvent[7c, 11d] may also lead to the higher activity. Carbon, ZrO_2, CeO_2, Al_2O_3 and MgO supports were much less effective than SiO_2 for activity of supported Ir-ReO_x. In terms of selectivity, all Ir-ReO_x catalysts except those on basic supports (CeO_2 and MgO) showed good selectivity to 1,3-PrD. Next, the influence of Ir amount with constant ratio of nominal Re/Ir (0.25) was investigated for Ir-ReO_x/Rutile catalyst (Figure 1B). A volcano-type dependency of glycerol conversion on Ir loading amount (2–8 wt%) was observed over Ir-ReO_x/Rutile, and the activity reached the maximum at Ir amout of 6 wt%. Similar volcano-type conversion tendency was also found in the optimization of Ir-ReO_x/SiO_2.[9b] However, such Ir-ReO_x/SiO_2 catalyst at Ir amount of 20 wt% gave higher activity, which is clearly larger than the optimized one (6 wt%-Ir) on rutile TiO_2, probably because of the higher S_{BET} of SiO_2 (485 m^2 g^{-1}) than rutile TiO_2 (6 m^2 g^{-1}). The reaction results over Ir-ReO_x/SiO_2 catalysts (4 wt%-Ir, Re/Ir = 1, and 20 wt%-Ir, Re/Ir = 1, nominal) which have been

reported to be very active are also shown in Figure 1B for comparison. In the case of SiO_2 supported Ir-ReO_x catalysts, our recent work suggested that higher Ir loading amount facilitated the formation of direct contact of neighboring Ir-ReO_x particles that possess more active site per Re amount.[9b] Here, the total Ir amount was set as the same (31 μmol) for all catalysts. The activity of Ir-ReO_x/Rutile (4–8 wt% Ir, Re/Ir = 0.25, nominal) was significantly higher than that of these Ir-ReO_x/SiO_2 catalysts. In addition to Ir-based activity, the amount of Re used in the preparation of Ir-ReO_x/Rutile catalysts was reduced to a quarter compared to those for Ir-ReO_x/SiO_2 (Ir: 4 or 20 wt%, Re/Ir = 1, nominal). To gain insight into the structure difference of Ir-ReO_x pairs on rutile TiO_2 and SiO_2 support, the Ir loading amount was fixed at 4 wt% in the following discussion to compare with other Ir-ReO_x catalysts including the previously reported 4 wt%-Ir Ir-ReO_x/SiO_2 (Re/Ir = 1, nominal).[7a-c, 9a] The activity over Ir-ReO_x/Rutile (4 wt%-Ir, Re/Ir = 0.25) was close to that of Ir-ReO_x/Rutile (6 wt%-Ir, Re/Ir = 0.25) which was the most active one at Ir amount from 2 to 8 wt% as shown in Figure 1B. As investigation of the effect of precursor of Ir, Ir-ReO_x/Rutile catalyst (4 wt%-Ir, Re/Ir = 0.25) was also prepared by using $Ir(NO_3)_4$ as precursor of Ir instead of H_2IrCl_6. The activity of the catalyst prepared with $Ir(NO_3)_4$ was much lower than that standard Ir-ReO_x/Rutile catalyst prepared with H_2IrCl_6, which can be due to the formation of larger particles using $Ir(NO_3)_4$ as discussed in the later section. This trend is different from that of Ir-ReO_x/SiO_2 catalysts where the catalytic performance was not changed by the use of different Ir precursors on catalyst preparation.[7c]

Next, the effect of nominal Re/Ir ratio over 4 wt%-Ir Ir-ReO_x/Rutile catalysts on glycerol hydrogenolysis was further examined as summarized in Table 1. Similarly to Ir/SiO_2 and ReO_x/SiO_2,[5b, 5e, 9b] both monometallic Ir/Rutile and ReO_x/Rutile cannot catalyze glycerol hydrogenolysis. The

glycerol conversion increased linearly with Re/Ir ratio between 0.06 and 0.25, and gradually saturated at higher Re/Ir ratio with a moderate decrease of 1,3-PrD selectivity. The promoting effect of sulfuric acid addition was also investigated over 4 wt%-Ir Ir-ReO_x/Rutile (Re/Ir = 0.25). Although the activity was slightly enhanced, it was different from the case of 4wt%-Ir Ir-ReO_x/SiO_2 (Re/Ir = 1), where the activity decreased significantly (ca. half) without addition of H_2SO_4.[5b, 7b] We recently found that the Re_2O_7 was prone to sublimate at relatively high loading amount on SiO_2 support during the calcination at 773 K.[9b] Given the much smaller S_{BET} of TiO_2 support, particularly for rutile TiO_2 (6 m^2 g^{-1}), the actual Ir and Re amounts were measured by XRF (Table 2). Overall, the actual amount of Ir on TiO_2 was almost the same as the nominal value. For ReO_x/Rutile catalyst, the actual Re amount was slightly lower than the nominal one (Table 2, entry 2). For those of Ir-ReO_x/Rutile catalysts (entries 3–7), the actual Re/Ir ratio was almost the same as the nominal one at the ratio between 0.06 and 0.25; however, it drastically stopped increasing at around 0.3 when the nominal ratio of Re to Ir exceeded 0.25. The loss of Re can be assigned to the Re_2O_7 sublimation on rutile TiO_2. The 4 wt%-Ir Ir-ReO_x/Rutile (Re/Ir = 0.25) prepared with $Ir(NO_3)_4$ precursor had also similar actual Re/Ir ratio (entry 8). For the catalyst with different Ir amount at fixed nominal Re/Ir ratio (0.25), sublimation of Re species was more likely to occur at higher Ir loading amount above 4 wt% (entries 9–11). As regard to Ir-ReO_x pairs supported on anatase and P25, it seems that Re species were easier to be sublimated on anatase than on rutile or P25 TiO_2 (entries 5, 13 and 15).

In the case of SiO_2 supported noble metals (Ir, Rh and Pt) with ReO_x modification catalysts, the iridium oxide was easier to reduce.[9a, 23] In addition, for noble metal catalysts on reducible supports including TiO_2, reduction temperature for pre-activation with H_2 is generally an important parameter.[24]

High reduction temperature favors the formation of strong metal–support interaction (SMSI), where suboxide (TiO_x) species may migrate and cover the surface of metal nanoparticles.[15b, 25] In some cases, SMSI much improves the catalytic performance, while in some cases the overlayer of these suboxide species blocks the access of reactants to the active site, giving negative effect on catalytic performance.[12a, 12b] Therefore, the effect of reduction temperature was investigated on a series of TiO_2 supported Ir-ReO_x catalysts. Table 3 lists the catalytic performance of Ir-ReO_x/TiO_2 reduced at various reduction conditions. The tested reduction conditions were liquid-phase reduction at 473 K, as the optimum reaction condition for Ir-ReO_x/SiO_2,[7b, 9b] and gas-phase reduction at 473, 573, 673 and 773 K (G, 473–773). The reduction at 773 K is the typical condition to induce SMSI for TiO_2-supported catalysts.[15a] Ir-ReO_x/Rutile and Ir-ReO_x/P25 catalysts showed similar trends for the change of reduction conditions. Gas-phase reduced catalysts (G, 473) showed higher activity than those reduced in liquid phase (L, 473). The activity was further increased when the reduction temperature in gas phase was increased to 573 K. After that, the activity was rather decreased with increase of reduction temperature. The selectivity was almost unchanged by the change of reduction conditions. These trends can be explained by the difference of reduction degree among the reduction temperature range of ≤573 K and the aggregation of metal particles and/or the covering of metal surface with TiO_x by SMSI above 573 K. The reduction behavior of Ir-ReO_x/Rutile will be explained in later section. In the case of Ir-ReO_x/Anatase, the activity was much lower than Ir-ReO_x/Rutile for all the tested reduction conditions. The (G, 473) catalyst showed the highest activity among Ir-ReO_x/Anatase catalysts, and the activity began to decrease at higher temperature (573 K). The 1,3-PrD selectivity over Ir-ReO_x/Anatase varied by the increase of reduction temperature: selectivity to 1,3-PrD decreased and that to 1,2-PrD increased

with increase of reduction temperature. These trends for activity and selectivity for Ir-ReO_x/Anatase were rather similar to those for Ir-ReO_x/SiO_2. The effects of reduction conditions imply that more active sites are available over rutile TiO_2 support for glycerol hydrogenolysis to 1,3-PrD, and these active sites can be stabilized over rutile TiO_2 other than SiO_2 or anatase supports. We selected Ir-ReO_x/Rutile (4 wt%-Ir, Re/Ir = 0.24*, (G, 573)) catalyst as the standard one because of better performance and almost no loss of Re species during calcinations (i.e. similar Re/Ir value of nominal (0.25) and actual ones (0.24*)). Although 4 wt%-Ir Ir-ReO_x/Rutile (Re/Ir = 0.30*, (G, 573)) catalysts showed higher activity, significant loss of Re was observed during calcination on this catalyst. We also tested the effect of the exposure to air after reduction. The 4 wt%-Ir Ir-ReO_x/Rutile (Re/Ir = 0.24*) was first reduced in the condition of (G, 573), and then passivated with 1 % O_2/He for 15 min at ambient temperature. This catalyst showed clearly lower activity than that without passivation (Table 3, entry 6), indicating that some species on rutile TiO_2 were easily oxidized even at low oxygen concentration.

Performance of Ir-ReO_x/Rutile catalyst. Table 4 gives the dependency of glycerol hydrogenolysis on reaction time over 4 wt%-Ir Ir-ReO_x/Rutile (Re/Ir = 0.24*). With reaction time prolonged, the conversion was steadily increased while 1,3-PrD selectivity decreased due to the overhydrogenolysis of 1,3-PrD to 1-propanol. The highest 1,3-PrD yield achieved by 4 wt%-Ir Ir-ReO_x/Rutile (Re/Ir = 0.24*) was 36% at 12 h with glycerol conversion of 69% and 52% selectivity to 1,3-PrD. This is a similar value to the one obtained over 4 wt%-Ir Ir-ReO_x/SiO_2 (Re/Ir = 1) + H_2SO_4 (38%).[7a] The Ir-ReO_x/Rutile is highly active in glycerol hydrogenolysis. The turnover frequency based on surface Ir^0 ((TOF_s = converted glycerol amount (mol) / {(total Ir amount (mol)) × 0.33 (CO adsorption [CO]/[Ir], Table 5) × 0.66 (Ir^0 ratio on the basis of FT-IR of adsorbed CO), Table S7) ×

reaction time (h)} was 830 h^{-1} over 4 wt%-Ir Ir-ReO_x/Rutile (Re/Ir = 0.24*), which was clearly higher than that achieved by 4 wt%-Ir Ir-ReO_x/SiO_2 (Re/Ir = 1) + H_2SO_4 (TOF_s: 370 h^{-1}) or 20 wt%-Ir Ir-ReO_x/SiO_2 (Re/Ir = 1) (450 h^{-1}).[9b] The initial productivity of 1,3-PrD of 4 wt%-Ir Ir-ReO_x/Rutile (Re/Ir = 0.24*) catalyst was 52 g g_{Ir}^{-1} h^{-1}, and the $P_{1,3\text{-PrD}}$ at highest yield was 17 g g_{Ir}^{-1} h^{-1} (Table 4). In the open literature as summarized in Table S1, the $P_{1,3\text{-PrD}}$ of SiO_2 supported Ir-Re alloy catalyst (Re/Ir = 1) was 7 g g_{Ir}^{-1} h^{-1} (40% conv. and 37% 1,3-PrD selectivity);[7d] Under similar reaction conditions, the $P_{1,3\text{-PrD}}$ was 18 g g_{Ir}^{-1} h^{-1} (initial one, at glycerol conversion of 20–25%) and 6 g g_{Ir}^{-1} h^{-1} (highest 1,3-PrD yield) over 4 wt%-Ir Ir-ReO_x/SiO_2 (Re/Ir = 1) + H_2SO_4,[7a, 7b] and 22 g g_{Ir}^{-1} h^{-1} (initial one) and 7 g g_{Ir}^{-1} h^{-1} (highest yield) over 20 wt%-Ir Ir-ReO_x/SiO_2 (Re/Ir = 1).[9b] Moreover, Yang's group has proposed the monometallic Ir/H-ZSM-5 as an effective catalyst for 1,3-PrD production in the absence of acid very recently.[26] The Ir^0-Ir^{3+} ratio as well as the Brønsted acid on the catalyst was correlated with the activity. However, harsh reaction conditions (453 K, 8 MPa H_2) were required to reach a maximum $P_{1,3\text{-PrD}}$ of 2 g g_{Ir}^{-1} h^{-1} at initial stage (29% conversion, 57% 1,3-PrD selectivity), which is much lower than Ir-ReO_x/Rutile catalysts. As far as we are concerned, the Ir-ReO_x/Rutile is the most active catalyst for glycerol hydrogenolysis to 1,3-PrD among the reported catalysts even with such a low Re/Ir ratio (0.24*) (Table S1).

The standard Ir-ReO_x/Rutile (Ir: 4 wt%, Re/Ir = 0.24*) was selected for kinetic study. The reaction order of H_2 was 0.9 (Figure 2A) which was close to the case of Ir-ReO_x/SiO_2 (about +1), suggesting the heterolytic dissociation of H_2 to produce proton (H^+) and hydride (H^-), and the hydride can be regarded as one active species in glycerol hydrogenolysis.[7b, 9b, 11b] Additionally, higher selectivity to 1,3-PrD (54% → 73%) was obtained with increasing H_2 pressure from 2 to 8 MPa at a similar glycerol

conversion level (11−16% conversion, Table S3). Furthermore, the influence of glycerol concentration on hydrogenolysis was investigated (Figure 2B and Table S4). The glycerol conversion rate (v_g) gradually increased with increasing glycerol concentrations from 5 to 50 wt%, and it became almost saturated at higher glycerol concentration (> 50 wt%). However, for Ir-ReO_x/SiO_2 catalysts (4 wt%-Ir and 20 wt%-Ir), the saturation was found at lower glycerol concentration (20 wt% glycerol).[5b, 7b, 9b] The glycerol concentration effect was influenced by the interaction between glycerol and catalyst, rather than changing the reaction mechanisms.[5b] Probably, the interaction between glycerol and the active site on Ir-ReO_x/Rutile is weaker than that on Ir-ReO_x/SiO_2, and high glycerol concentration is required to reach saturation. The reaction order on glycerol concentration around standard reaction conditions (67 wt% glycerol solution) was about 0.2 (Figure S1), suggesting that the coverage of glycerol adsorption on the catalyst surface is almost saturated under the standard reaction conditions. Another important point was the high 1,3-PrD selectivity (about 70%), which showed independency of glycerol concentrations (10−80 wt%). Similar behavior was also observed over 20 wt%-Ir Ir-ReO_x/SiO_2 catalyst.[9b] It is noteworthy that an obvious decline of activity was found when no water solvent (100 wt% glycerol solution) was added (Figure 2B). We have discussed the plausible formation way of Re−OH site that was regarded as the adsorption site for glycerol rather than serving as acid, and this site was formed by activation of water molecules on ReO_x cluster with low valence attached to Ir metal.[9b] Previous Ir-ReO_x/SiO_2 system was optimized by liquid-phase reduction (L, 473), and the presence of water during pre-reduction treatment makes it difficult to provide more evidences for this assumption. On the contrary, the Ir-ReO_x/Rutile was optimized by gas-phase reduction at higher temperature (G, 573). The lower activity without addition of water can be explained by the absence of

water molecules available for activation on ReO_x cluster to form Re–OH site for glycerol adsorption. Since the glycerol hydrogenolysis also produces water, further work is required to clarify the role of water in glycerol hydrogenolysis over metal oxide modified bimetallic catalysts. Overall, the reaction mechanism around the standard conditions is essentially the same to the cases of 4 wt%-Ir Ir-ReO_x/SiO_2 (Re/Ir = 0.83*) + H_2SO_4 and 20 wt%-Ir Ir-ReO_x/SiO_2 (Re/Ir = 0.34*) system: Glycerol was adsorbed on ReO_x cluster at the 1-position to form terminal alkoxide. Meanwhile the H_2 heterolytically dissociated on the Ir metal surface producing the hydride to attack the alkoxide at 2-position, cleave the C–O bond, and release the 1,3-PrD by hydrolysis of the reduced alkoxide.[7b, 9b]

Next, the reusability of 4 wt%-Ir Ir-ReO_x/Rutile was investigated. First, the catalysts were collected under N_2 atmosphere, washed with deionized water which was stored under air, and then used for the next run. The activity of both catalysts was gradually decreased with repeated usage (Table S5). However, the Ir and Re amount over both used catalysts was the same to the fresh catalyst as determined by XRF (0.24* → 0.24*; 0.30* → 0.31* after first run use) as well as very low leached Ir and Re amount over these catalysts (Ir: <0.2% and Re: <0.3%, based on actual amount of metal over catalyst), indicating that metal leaching was not the main cause for activity decrease. Then another test was carried in which the water solvent for washing was further degassed to remove any residual oxygen. After four times usage, both the high activity and 1,3-PrD selectivity was maintained, giving good reusability of Ir-ReO_x/Rutile (4 wt%-Ir, Re/Ir = 0.24*) under this strict O_2-free environment (Table 6). This behavior is different from high loading Ir-ReO_x/SiO_2 (Ir: 20 wt%, Re/Ir = 0.34*) since the SiO_2 supported Ir-ReO_x pairs could be reused when only the gas phase was O_2-free.[9b] It indicates that the Ir-ReO_x active species are less stable to oxidation on rutile TiO_2 rather than those on SiO_2 support,

which was further examined by XPS measurement in the later discussion.

Characterization of Ir-ReO_x/Rutile and related catalysts. H_2-TPR was performed to determine the reducibility of those catalysts prepared with different Ir precursors, Re/Ir ratios, and crystalline phases of TiO_2 (Figures 3 and S2). The ReO_x/Rutile (0.7 wt%) showed a small single reduction peak between 400–500 K, which temperature range was clearly lower than that (550–700 K) on ReO_x/SiO_2.[7b, 9b] The total H_2 consumption corresponded to the partially reduced ReO_x species on rutile TiO_2 to the valence of +2 (Table S6). Two main peaks were observed for both Ir/Rutile and Ir-ReO_x/Rutile. The Ir/Rutile was gradually reduced at a wide range of temperature (350–800 K), suggesting the incomplete reduction for Ir/Rutile at 573 K. The reduction was promoted significantly as the reduction peaks became narrow and shifted to lower temperature with increasing the Re addition amount. The reduction was almost completed at 573 K with Re/Ir ratio ≥ 0.24. It agrees well with the optimization reduction temperature (573 K) of Ir-ReO_x/Rutile (Re/Ir = 0.24* and 0.3*) for catalytic activity as discussed in earlier section. The average valence of Re was calculated to be +1.5~+3.5 on Ir-ReO_x/Rutile catalysts (Table S6). The range of reduction temperature of Ir-ReO_x/Rutile by the use of $Ir(NO_3)_4$ as Ir precursor was similar to the standard (H_2IrCl_6 precursor), with a small difference of curve shape (Figure 3). In addition to rutile TiO_2 supported Ir-ReO_x catalysts, the reducibility of anatase and P25 TiO_2 based catalysts is also shown in Figure S2. The pure TiO_2 supports presented no obvious reduction peak, and the promotion effect of reduction of Ir with small amount of Re addition was also observed on Ir-ReO_x/Anatase and Ir-ReO_x/P25. The average valence of Re on Ir-ReO_x/TiO_2 (4wt%, Re/Ir = 0.25) calculated with the assumption of complete IrO_2 reduction to Ir and no TiO_2 reduction, decreased in the following order: Ir-ReO_x/Rutile (+6.2, precursor of $Ir(NO_3)_4$) > Ir-

ReO_x/P25 (+4.3) > Ir-ReO_x/Rutile (+2.5) > Ir-ReO_x/Anatase (+1.0) (Table S6). However, there was the existence of partially reduced rutile TiO_2 support. For the Ir/Anatase and Ir/P25, the calculated H_2 consumption amount based on actual Ir amount ($IrO_2 + 2H_2 \rightarrow Ir + 2H_2O$) was consistent with that determined by TPR. However, the value of consumed H_2 amount by TPR measurement (44.15 μmol) on Ir/Rutile was slightly larger than the theoretical one (20.81 μmol Ir, 41.62 μmol), indicating the presence of Ir promoted the reduction of TiO_2 (Table S6). Therefore, it can be deduced that some amount of rutile TiO_2 also consumed H_2 in TPR measurement for those Ir-ReO_x/Rutile catalysts, and the Re valence determined by TPR cannot accurately correspond to the actual Re oxidized state.

The particle size of various Ir/TiO_2 and Ir-ReO_x/TiO_2 catalysts after reduction (G, 573) was measured by TEM (Figure 4). The average particle size of monometallic iridium (4 wt%) on TiO_2 decreased in order: Ir/Anatase (6.6 nm) > Ir/P25 (2.8 nm) ≅ Ir/Rutile (2.6 nm). The high dispersion of Ir on rutile TiO_2 can be explained by the interfacial lattice matching of IrO_2 (rutile structure) and rutile TiO_2 (lattice constant of IrO_2: $a = b = 0.450$ nm, $c = 0.315$ nm and rutile TiO_2: $a = b = 0.459$ nm, $c = 0.296$ nm),[17a] which favors the formation of Ir-O-Ti bond for Ir species anchored during impregnation and calcination. With addition of small amount of Re (Re/Ir = 0.25), the promotion effect on the dispersion of particles was observed over all the Ir-ReO_x/TiO_2 catalysts. The Ir-ReO_x pairs demonstrated higher dispersion on rutile TiO_2 (1.9 nm) than that on P25 (2.5 nm) or anatase (5.3 nm). Additionally, those particles were preferentially to locate on the rutile TiO_2 rather than anatase surface because P25 was a mixture of anatase and rutile TiO_2 (weight ratio of 4:1) and the particles were countable on only a few regions on bulk TiO_2 (Figure 4F). Combined with catalytic performance on Ir-ReO_x supported over rutile TiO_2, anatase and P25 (Figure 1A), we suggested that both dispersion of

Ir particles and interaction between Ir-ReO_x should be taken into consideration to understand the activity difference over TiO_2 supported Ir-ReO_x catalysts. The location of Ir particles and Re species on TiO_2 support may be more important. Some Re species on anatase TiO_2 were probably mainly located distant from Ir particles on the surface of support, which results in no activity for glycerol hydrogenolysis. For P25 support, some Re species were present on the crystallites of anatase that cannot be interacted with Ir particles since the activity over Ir-ReO_x/P25 was clearly lower than that over Ir-ReO_x/Rutile and the average Ir particle size of Ir-ReO_x supported over P25 (2.5 nm) and rutile TiO_2 (1.9 nm) was comparable (Figures 4E and F). In addition, small particle size with narrow distribution was also observed on 4 wt%-Ir Ir-ReO_x/Rutile (Re/Ir = 0.30*) (1.8 nm, Figure S3). The particle size increased with higher Ir loading amount at fixed Re/Ir (0.25) (Figure S4). Another important point is the surface density of Ir particles on Ir/Rutile and Ir-ReO_x/Rutile catalysts: the surface of rutile TiO_2 particles was almost totally covered with Ir particles. In the case of 4 wt%-Ir Ir-ReO_x/Rutile (Re/Ir = 0.25) prepared by $Ir(NO_3)_4$ precursor, large particles were observed with wide size distribution (3.7 nm, Figure S5). The standard catalyst of 4 wt%-Ir Ir-ReO_x/Rutile (Re/Ir = 0.24*) reduced at high temperature (773 K) showed slightly larger particle size (2.1 nm) (Figure S6) compared to that reduced at 573 K (1.9 nm).

Figure 5 presents the XPS results for Ir/Rutitle, Ir-ReO_x/Rutile (Re/Ir = 0.24*), Ir-ReO_x/Rutile (Re/Ir = 0.30*) catalysts after reduction, and Ir-ReO_x/Rutile (Re/Ir = 0.24*) after reduction and passivation. The surface valence of Ir and Re and the fitting results are summarized in Tables 6 and 7, respectively. The Ir 4f signals over these catalysts were deconvoluted into a complex of Ir^0, Ir^{3+}, and Ir^{4+} species. The main peak of Ir $4f_{7/2}$ binding energy (BE) value at 60.6–61.1 eV was assigned to Ir^0

species[27] (Figure 5A, B, C, and D, and Table 7), with Ir^{3+} species at peak position 61.7–62.2 eV,[12e] and Ir^{4+} species at peak position 62.7–63.2 eV.[27] The fitting validity can be confirmed by the TPR results for Ir/Rutile that the Ir species were not fully reduced at 573 K. For SiO_2 supported Ir-ReO_x catalysts, a typical reduction temperature at 473 K was sufficient for all the Ir species reduced to metallic state, and no signals for Ir^{3+} and Ir^{4+} species can be detected in XPS measurement.[5b, 11h] The presence of surface $Ir^{\delta+}$ species can be due to the small amount of oxidized Ir species strongly bonded to rutile TiO_2. In addition, the reduction of surface Ir species was promoted by Re modifier since the proportion of Ir^0 increased from about 70% to 80% with decreasing the amount of Ir^{3+} and Ir^{4+} complex (Table 7). A positive shift of Ir peak position (about 0.5 eV) to higher BE value was found on Ir-ReO_x/Rutile in comparison with Ir/Rutile. Such shift was not ascribed to the energy calibration error because the Ti^{4+} $2p_{3/2}$ showed similar peak position (~458.8 eV,[28] Figure S7) over these samples. It can be explained by the electronic interaction between Ir and ReO_x on rutile TiO_2 surface, where electrons were transferred from Ir species to Re^{n+} to stabilize ReO_x at intermediate valence (mainly +3 as shown later). It can be also supported by the fact that FT-IR spectra of adsorbed CO over Ir-ReO_x/Rutile appeared at higher wavenumber than that over Ir/Rutile as discussed in the section below. With respect to Re 4f signals over related catalysts, it also demonstrates different surface oxidized state of Re species than that over Ir-ReO_x/SiO_2 as discussed below. Additional two peaks of Ti 3p at BE value of 38.0 eV[29] and Ir $5p_{3/2}$ of 48.5 eV[30] were detected on all the Ir-ReO_x/Rutile samples. In the case of Ir-ReO_x/Rutile catalysts (G, 573) at Re/Ir ratio of 0.24* and 0.30*, two peaks at BE value of 41.7 and 42.5 eV were set for raw spectra of Re $4f_{7/2}$ fitting. The first main peak can be assigned to Re^{3+} species, which was rarely observed over SiO_2 supported Ir-ReO_x catalysts (typically a variety of Re species at

0, +2, +4, +6, and +7 over Ir-ReO_x/SiO_2),[5b, 11g, 11h] but available over other bimetallic catalysts such as Pd-Re,[29, 31] Ru-Re[32] and Rh-Re catalyst.[33] The second smaller peak was ascribed to Re^{4+} species (Figure 5E and F, and Table 7). On both catalysts, about 80% of Re species were found to be at the oxidized state of +3 with the rest of Re species at +4 (Table 7). Those different surface states of Ir (slightly oxidized) and ReO_x (mostly stabilized at +3) stabilized on rutile TiO_2 indicates the unique advantage of using rutile TiO_2 as a support than inert SiO_2 support. Another important point is the oxidized state of Re after passivation. Although the surface composition of Ir over Ir-ReO_x/Rutile (Re/Ir = 0.24*) after passivation was similar to the corresponding catalyst after reduction, about half amount of Re species (Re^{3+} and Re^{4+}) were oxidized to Re^{7+} after exposure to carrier gas with low oxygen concentration (1% O_2/He) (Table 7). Therefore the Re species (Re^{3+} and Re^{4+}) were sensitive to oxygen, and can be easily oxidized even in the presence of small amount of oxygen. The possible deactivation mechanism for Ir-ReO_x/SiO_2 was assigned to the coverage of Re^{n+} species on Ir metal surface after exposure to oxygen atmosphere.[9b] Some Re^{n+} species were prone to be oxidized to Re^{7+}, which has high solubility in water, and readsorbed on the surface of Ir particles. It can explain the observed decrease of activity both in the repeated usage when the O_2 in water solvent was not totally removed (Table S5), and for catalyst after passivation (Table 3, entry 6). The surface atom ratio of Re_s/Ir_s calculated by XPS measurement is also presented in Table 7. These values were close to the actual ratio determined by XRF. Therefore, the Ir and Re valence can be determined from the XPS fitting results on the basis of the assumption that all the Ir and Re species are detectable in XPS measurement. Moreover, the accurate amount of Ti^{3+} species was particularly difficult to calculate when combined with rich Ti^{4+} species.[28] In our analyses of XPS results, the surface Ti species were

mainly Ti^{4+} on rutile TiO_2 with only about 4% of Ti^{3+} species over 4 wt%-Ir catalysts at Re/Ir ratio of 0.24* and 0.30* after reduction (Figure S7).

In order to further determine the surface state of Ir and Re, FT-IR of adsorbed CO combined with CO adsorption was performed (Figure 6). No peak of adsorbed CO on ReO_x/Rutile was detected (data not shown here). A strong peak at 2083~2089 cm^{-1} was observed on Ir-ReO_x/Rutile catalysts (Figure 6A). Generally, ReO_x cannot absorb CO molecules,[7b] and the peak position of CO molecule adsorbed on Ir metal was about 2066~2069 cm^{-1} (linear adsorption of CO) for Ir-ReO_x/SiO_2[7b, 7d, 34] and that on Re metal surface was 2030~2050 cm^{-1}.[35] Therefore, the shift of the former peak to higher wavenumber can be explained by the presence of $Ir^{\delta+}$ (Ir^{3+} and Ir^{4+}) species on Ir metal surface. As a result, the Ir atoms became cationic, which was consistent with the XPS results. We further separated the peak at wavenumber range of 2030~2110 cm^{-1} by two peaks (Figure 6B and Table S7). The former peak at higher wavenumber (2083~2089 cm^{-1}) was assigned to the linearly adsorbed CO on $Ir^{\delta+}$ species, which also has been observed with strong intensity (~2090 cm^{-1}) on partially oxidized $Ir^{\delta+}$ species over Ir-Au/P25, Ir-Au/Al_2O_3 and Ir-Ag/Al_2O_3.[36] Particularly, for those Au-Ir/Al_2O_3 and Ag-Ir/Al_2O_3 samples, the partially oxidized Ir species (Ir^0 with Ir^{3+} and Ir^{4+} complex as confirmed by XPS) on these catalysts surface after reduction showed similar vibrations position of linearly adsorbed CO on $Ir^{\delta+}$ as the case of that on Ir-ReO_x/Rutile.[36c, 36d] The latter peak at lower position (2070~2076 cm^{-1}) was linearly adsorbed CO on Ir metal (Table S7). The area ratio of CO adsorbed on $Ir^{\delta+}$ to Ir metal was close to the XPS fitting results (Table 7). It seems that the Ir-ReO_x/Rutile catalyst with lower Ir loading amount (2 wt%) is prone to be oxidized because higher proportion of $Ir^{\delta+}$ species was suggested on 2 wt%-Ir catalysts (Table S7). Moreover, the less active catalyst with lower Ir loading amount (2 wt%-Ir) showed

same peak position (2083 cm^{-1}) as the case of monometallic Ir/Rutile catalyst. This result suggests that the local structure of catalyst with lower loading amount (2 wt%-Ir) was different from those catalysts with higher Ir loading amount.

XAS analyses were performed with Ir/Rutile and Ir-ReO_x/Rutile catalysts after reduction or catalytic use. The valence of Ir was determined from Ir L_3-XANES spectra using the intensity of white line, and the results also supported the presence of $Ir^{\delta+}$ species for all the examined catalysts after reduction (G, 573) or reaction (Figures S8(I)), which was consistent with TPR, XPS, and FT-IR of adsorbed CO results. The calcined Ir-ReO_x/Rutile (Ir: 4 wt%, Re/Ir = 0.24*) showed similar spectrum to that of IrO_2. The Ir L_3-edge EXAFS analysis results are shown in Table 8 (the raw EXAFS spectra are shown in Figure S9). The presence of Ir-O shell indicates the incomplete reduction of Ir species over rutile TiO_2 supported catalysts (Table 8, entries 1–12) in contrast to the fully reduced Ir metal on Ir-ReO_x/SiO_2 after reaction (entry 13). For the Ir/Rutile and Ir-ReO_x/Rutile catalysts after reduction or reaction, similar fitting results including the number of shells, coordination number (CN), and bond distance were obtained (entries 1–6), suggesting that the local structure was similar over catalysts after reduction or reaction. The CN of Ir-Ir (or -Re) bond was about 9 for the 4 wt%-Ir Ir-ReO_x/Rutile catalysts at various Re/Ir ratio (entries 3–9) with bond distance of 0.274–0.275 nm. The CN of Ir-Ir (or -Re) bond was increased from about 8 to 10 when Ir loading amount increased from 2 wt% to 8 wt% at nominal Re/Ir ratio of 0.25 (entries 3, and 10–12) with same bond distance of 0.274 nm. This increasing of CN tendency can be explained by larger particles on catalysts with higher Ir loading amount which was verified by TEM results. The Ir-ReO_x pairs on rutile TiO_2 even with lower Re/Ir ratio (Ir: 4 wt%) were in higher dispersion than SiO_2 supported Ir-ReO_x pairs with higher Re/Ir ratio

since the lower CN of Ir-Ir (or -Re) was suggested by curve fitting results. An interesting point was the decrease of Ir-O bond distance after monometallic Ir/Rutile modified by Re. The bond distance of Ir-O decreased from about 0.212 nm on Ir/Rutile to 0.203 nm on Ir-ReO_x/Rutile, suggesting the addition of Re increased the affinity between Ir and oxygen in a local region.

The Re L_3-XANES spectra are shown in Figure S8(II) and (III), and the results of EXAFS analysis are shown in Table 9 (the raw EXAFS spectra are shown in Figures S10). Similar valence of Re over 4 wt%-Ir Ir-ReO_x/Rutile (Re/Ir = 0.24*) after calcination to NH_4ReO_4 (Re precursor) confirmed the accuracy of white line intensity method. The average valence of Re was determined to be about +3 for all the examined Ir-ReO_x/Rutile catalysts, typically shown in Figure S8(III). This valence was similar to the case of Ir-ReO_x/SiO_2 + H_2SO_4 (Ir: 4 wt%) after reaction,[7b] but higher than the high loading amount Ir-ReO_x/SiO_2 (Ir: 20 wt%, Re/Ir = 0.34*) catalyst in the absence of H_2SO_4 after reaction (+1.1).[9b] There is no clear relationship between the average Re valence and catalytic performance. Based on analyses of Re L_3-edge EXAFS in Table 9 (entries 1–10), the presence of Re-O bond with CN from 0.5 to 1.1 was suggested over the tested catalysts, indicating that the Re species are partially oxidized on catalysts after reduction or reaction. The bond distance of Re-O (0.211–0.212 nm) over rutile TiO_2 supported catalysts was shorter than that (0.202–0.203 nm) of SiO_2 supported 4 wt%-Ir Ir-ReO_x catalyst,[7a, 7b] which has also been observed over 20 wt%-Ir Ir-ReO_x/SiO_2 (Re/Ir = 0.34*) catalyst.[9b] It is likely that the single bond of Re-O is more abundant on both Ir-ReO_x/Rutile and 20 wt%-Ir Ir-ReO_x/SiO_2 than that on 4 wt%-Ir Ir-ReO_x/SiO_2. With respect to the bond distance of Re-Re (or -Ir), it was similar for those catalysts regardless of support (rutile TiO_2 and SiO_2) or composition of catalysts (0.263–0.268 nm). Compared to the bond distance of Ir-Ir (or -Re) (0.274–0.275 nm), the

shorter bond distance (0.263–0.268 nm) suggests the absence of Ir-Re alloy, which is in agreement with other characterization results (CO FT-IR and XPS). An important point was the CN of Re-Re (or -Ir), which to some extent can reflect the strength of Ir-ReO_x interaction. Our very recent work suggested that the Ir-ReO_x interaction can be enhanced by increasing the Ir loading amount up to 20 wt% on SiO_2.[9b] In that case, slight larger ReO_x clusters were stabilized and attached to neighboring Ir metal surface with an increase of CN of Re-Re (or -Ir) from 6.2 (4 wt%-Ir Ir-ReO_x/SiO_2, Re/Ir = 0.83*) to 8.6 (20 wt%-Ir Ir-ReO_x/SiO_2, Re/Ir = 0.34).[9b] Higher CN of Re-Re (or -Ir) was also obtained on rutile TiO_2 supported catalysts except 2 wt%-Ir Ir-ReO_x/Rutile. The CN of Re-Re (or -Ir) over 2 wt%-Ir Ir-ReO_x/Rutile catalyst was similar to the 4 wt%-Ir Ir-ReO_x/SiO_2 (entries 8 and 11), but lower than that over other Ir-ReO_x/Rutile catalysts. In addition, the fitting results of corresponding catalysts after reduction or reaction (entries 1–4) were similar, indicating that such stable structure can be maintained after catalytic use.

Relationship between activity and catalyst structure in glycerol hydrogenolysis to 1,3-PrD over Ir-ReO_x/Rutile. On the basis of the discussion of activity and characterization results above, the relationship between the catalytic performance and structure was further clarified. The average valence of both Ir and Re determined by different method is summarized in Table 5, and those results are consistent except the Re valence calculated by TPR (Table S6). The disagreement can be due to the incomplete reduction of Ir species, and partially reduced TiO_2 which was catalyzed by noble metal as we discussed in earlier section. The results of XPS and XANES analyses for Re valence were similar, and we think that XPS and XANES reflected the exact Re valence. Here the glycerol conversion was fixed at 20–25% to compare the 1,3-PrD productivity ($P_{1,3\text{-PrD}}$) over various Ir-ReO_x/Rutile catalysts

with different compositions (Figure 7 and Table 5). The increasing tendency of $P_{1,3\text{-PrD}}$ correlated to the Ir loading amount with similar trend of CN of Re-Re (or -Ir) change in the range of 2–6 wt%, and then it decreased slightly at higher Ir loading amount with higher CN of Re-Re (or -Ir) (Figure 7A). Then we considered the relationship between the activity and surface ratio of $Ir^{\delta+}/(Ir^{\delta+}+Ir^{0})$ which was determined from fitting results of CO FT-IR (Table S7). If the $Ir^{\delta+}$ species were directly involved in the glycerol hydrogenolysis, the activity over 2 wt%-Ir Ir-ReO_x/Rutile should be higher than those catalysts with higher Ir loading amount since smaller particles (TEM and EXAFS) and more $Ir^{\delta+}$ species (CO FT-IR) were suggested on 2 wt%-Ir catalyst. The lower activity over Ir-ReO_x/Rutile at lower Ir loading amount excludes the direct participation of $Ir^{\delta+}$ species during the hydrogenolysis reaction. We further calculated the coverage ratio of ReO_x on Ir metal surface (Table 5), and coverage ratio (62~67%) was almost independent of Ir loading amount on rutile TiO_2. The density of surface Ir^0 on rutile TiO_2 (Ir loading amount / 192.2 × N_A × D_{CO} × Ir^0 ratio (determined from CO FT-IR) / S_{BET} of rutile TiO_2) decreased in order: 8 wt%-Ir Ir-ReO_x/Rutile (5.4/nm^2) > 6 wt%-Ir (4.7/nm^2) > 4 wt%-Ir (4.4/nm^2) > 2 wt%-Ir (2.4/nm^2), which correlated with $P_{1,3\text{-PrD}}$ value over catalysts at Ir amount from 2 to 6 wt% as plotted in Figure 7A. The lower $P_{1,3\text{-PrD}}$ over 8 wt%-Ir Ir-ReO_x/Rutile was attributed to the larger particle size (3.0 nm, Figure S4). On the other hand, similar kinetic results on 4 wt%-Ir Ir-ReO_x/Rutile (Re/Ir = 0.24*) and SiO_2 supported Ir-ReO_x catalysts (reaction order on H_2 about 1 and reaction order on glycerol concentration about 0 under standard reaction conditions) suggest that rutile TiO_2 is not directly involved in this reaction. Therefore the active site on Ir-ReO_x/Rutile is the Ir-ReO_x interface and the activity showed dependency on the structure of Ir and Re species. In the case of 4 wt%-Ir catalysts with different Re/Ir ratio (Figure 7B), slightly higher ratio gives higher surface ratio

of Re to Ir. The $P_{1,3\text{-PrD}}$ significantly increased from 52 to 94 g g_{Ir}^{-1} h^{-1} with Re/Ir ratio increasing from 0.24* to 0.30* (surface ratio: 0.16 → 0.25, Table 7), indicating that the structure of these two catalysts is different although the XAS analysis results give similar local coordination environment. The activity result can be explained by the increase of surface Re concentration to create more active sites available on catalyst surface. Similar activity dependency on surface Ni concentrations has also been suggested over Ni@TiO_{2-x} catalyst.[25] The IrO_x species on the bottom of Ir particles can be strongly interacted with the ground layer of rutile TiO_2, considering the similar structure of IrO_2 and rutile TiO_2, and the XPS result of small amount of partially reduced TiO_2 as shown in Figure 8. The role of rutile TiO_2 is serving as stabilization of small Ir nanoparticles with uniform and high dispersion even modified with low amount of Re. In the case of SiO_2 support (4 wt%-Ir), the dispersion of Ir-ReO_x particles was promoted at higher Re/Ir ratio (typical ratio of 0.83*), and the average particle size of 4 wt%-Ir Ir-ReO_x/SiO_2 (Re/Ir = 0.83*) was in a wide range of distribution (1.5–6.5 nm).[9b] For catalysts with lower Ir amount after reduction, the Ir-ReO_x pairs are highly dispersed on rutile TiO_2, and non-contact of Ir particles is suggested with more oxidized Ir species (IrO_x) located on the interface between of Ir particles and rutile TiO_2 surface as illustrated in Figure 8A. This structure is supported by EXAFS result (low CN of Re-Re or (-Ir) as the case of 4 wt%-Ir Ir-ReO_x/SiO_2) and CO FT-IR (higher proportion of $Ir^{\delta+}$ species). Thanks to the low surface area of rutile TiO_2 (S_{BET} 6 m^2 g^{-1}), direct contact of particles are formed on slightly higher Ir loading amount with low Re/Ir ratio (Figure 8B). Based on the Ir particle size, the surface area per one Ir-ReO_x particle (S_{BET} of rutile TiO_2 / (Ir loading amount / 192.2 × N_A / total Ir atoms per one Ir particle) is calculated to be 9.6, and 16.2 nm^2/one particle for 4 wt%-Ir (1.9 nm, ~201 total Ir atoms per one Ir particle by assuming a cuboctahedron structure of Ir

particles[9a]) and 2 wt%-Ir catalyst (1.6 nm, ~169 total Ir atoms per one Ir particle), respectively. The Ir particles in 4 wt%-Ir catalyst are prone to have contact with each other as shown in Figure 8. Such structure increases the number of active site (Ir-ReO_x interface) per Re amount by locating some of Re species between Ir particles. In fact, higher CN of Re-Re or (-Ir) was suggested by EXAFS analysis. The Re species on contact site between Ir particles is one of the main active sites over higher loading Ir-ReO_x/Rutile. Such sites may have more sterically hindered than the Ir-ReO_x interface over 4 wt%-Ir Ir-ReO_x/SiO_2 with non-contact site, and this effect can induce the weaker interaction between glycerol and the active site as observed by the effect of glycerol concentration on the reaction rate.

4. Conclusions

The Ir-ReO_x pairs with actual low Re/Ir ratio (denoted by asterisk (*)) were highly dispersed on rutile TiO_2. Compared to 4 wt%-Ir Ir-ReO_x/SiO_2 (Re/Ir = 1, (0.83*)) + H_2SO_4 system, about threefold and fivefold enhancement in $P_{1,3\text{-PrD}}$ for glycerol hydrogenolysis to 1,3-PrD was achieved over 4 wt%-Ir Ir-ReO_x/Rutile catalysts in the absence of H_2SO_4 at Re/Ir ratio of 0.24* and 0.30*, respectively. The $P_{1,3\text{-PrD}}$ over 4 wt%-Ir Ir-ReO_x/Rutile (Re/Ir = 0.25, (0.24*)) was also about 2.5 times higher than the previously reported 20 wt%-Ir Ir-ReO_x/SiO_2 (Re/Ir = 1, (0.34*)) which had been the most active catalyst for glycerol hydrogenolysis to 1,3-PrD. The highest yield of 1,3-PrD was 36% over 4 wt%-Ir Ir-ReO_x/Rutile (0.24*) for 12 h, which was similar to the value (38%) accomplished by 4 wt%-Ir Ir-ReO_x/SiO_2 (Re/Ir = 0.83*) + H_2SO_4 system for 36 h under same reaction conditions. The proposed structure of 4 wt%-Ir Ir-ReO_x/Rutile (0.24*) was responsible for the much enhanced activity: high surface density of uniform Ir particles on rutile TiO_2 were covered with ReO_x cluster (average valence of Re: +3), which favors the formation of direct contact site and increased the number of active Ir-

ReO_x interface. Similar structure of IrO_2 and rutile TiO_2 might enable the high surface density of very small Ir particles on low surface area rutile TiO_2. In addition, the rutile TiO_2 supported Ir-ReO_x catalyst was sensitive to oxygen since Re^{n+} species were easy to be oxidized to +7, destabilizing the active site, and thus decreasing the activity. The Ir-ReO_x/Rutile catalyst is reusable without the loss of activity or selectivity; however, the reuse of this catalyst ought to be strictly conducted without exposure to air (N_2 atmosphere and degassed water solvent).

This investigation highlights the critical role of support in preparation of bimetallic catalysts, and how the physical parameters (loading amount/metal ratio) tune the bimetallic catalyst structures and thus affect the activity. It may also provide new avenues to exploit the affinity between Ir and rutile TiO_2 in construction of Ir based bimetallic catalysts on rutile TiO_2.

Supporting Information

Materials and kinetics results

Comparison of glycerol hydrogenolysis to 1,3-propanediol performance

Characterization results including TPR, TEM, XRF, XPS, XAS and FT-IR of adsorbed CO

Acknowledgements

Part of this work was supported by JSPS KAKENHI 18H05247. Lujie Liu acknowledges financial support from the China Scholarship Council (CSC). We also thank the Technical Division in the School of Engineering in Tohoku University for their assistance in TEM and XPS measurements.

References

(1) (a) Corma, A.; Iborra, S.; Velty, A. Chemical Routes for the Transformation of Biomass into Chemicals. *Chem. Rev.* **2007,** *107*, 2411–2502. (b) Besson, M.; Gallezot, P.; Pinel, C. Conversion of

Biomass into Chemicals over Metal Catalysts. *Chem. Rev.* **2014,** *114*, 1827–1870. (c) Serrano-Ruiz, J. C.; Luque, R.; Sepulveda-Escribano, A. Transformations of Biomass-Derived Platform Molecules: From High Added-Value Chemicals to Fuels via Aqueous-Phase Processing. *Chem. Soc. Rev.* **2011,** *40*, 5266–5281.

(2) (a) Zhou, C. H. C.; Beltramini, J. N.; Fan, Y. X.; Lu, G. Q. M. Chemoselective Catalytic Conversion of Glycerol as a Biorenewable Source to Valuable Commodity Chemicals. *Chem. Soc. Rev.* **2008,** *37*, 527–549. (b) Katryniok, B.; Paul, S.; Belliere-Baca, V.; Rey, P.; Dumeignil, F. Glycerol Dehydration to Acrolein in the Context of New Uses of Glycerol. *Green Chem.* **2010,** *12*, 2079–2098. (c) Pagliaro, M.; Ciriminna, R.; Kimura, H.; Rossi, M.; Della Pina, C. From Glycerol to Value-Added Products. *Angew. Chem. Int. Ed.* **2007,** *46*, 4434–4440. (d) Sun, D.; Yamada, Y.; Sato, S.; Ueda, W. Glycerol Hydrogenolysis into Useful C3 Chemicals. *Appl. Catal. B* **2016,** *193*, 75–92.

(3) Garcia-Sancho, C.; Cecilia, J. A.; Merida-Robles, J. M.; Gonzalez, J. S.; Moreno-Tost, R.; Infantes-Molina, A.; Maireles-Torres, P. Effect of the Treatment with H_3PO_4 on the Catalytic Activity of Nb_2O_5 Supported on Zr-Doped Mesoporous Silica Catalyst. Case Study: Glycerol Dehydration. *Appl. Catal. B* **2018,** *221*, 158–168.

(4) (a) Ketchie, W. C.; Murayama, M.; Davis, R. J. Selective Oxidation of Glycerol over Carbon-Supported AuPd Catalysts. *J. Catal.* **2007,** *250*, 264–273. (b) Katryniok, B.; Kimura, H.; Skrzynska, E.; Girardon, J. S.; Fongarland, P.; Capron, M.; Ducoulombier, R.; Mimura, N.; Paul, S.; Dumeignil, F. Selective Catalytic Oxidation of Glycerol: Perspectives for High Value Chemicals. *Green Chem.* **2011,** *13*, 1960–1979.

(5) (a) Sun, Q. H.; Wang, S.; Liu, H. C. Selective Hydrogenolysis of Glycerol to Propylene Glycol on Supported Pd Catalysts: Promoting Effects of ZnO and Mechanistic Assessment of Active PdZn Alloy Surfaces. *ACS Catal.* **2017,** *7*, 4265–4275. (b) Varghese, J. J.; Cao, L.; Robertson, C.; Yang, Y.; Gladden, L. F.; Lapkin, A. A.; Mushrif, S. H. Synergistic Contribution of the Acidic Metal Oxide–Metal Couple and Solvent Environment in the Selective Hydrogenolysis of Glycerol: A Combined Experimental and Computational Study Using ReO_x–Ir as the Catalyst. *ACS Catal.* **2019,** *9*, 485–503. (c) Nakagawa, Y.; Tomishige, K. Heterogeneous Catalysis of the Glycerol Hydrogenolysis. *Catal. Sci. Technol.* **2011,** *1*, 179–190. (d) Nakagawa, Y.; Tamura, M.; Tomishige, K. Catalytic Materials for the Hydrogenolysis of Glycerol to 1,3-Propanediol. *J. Mater. Chem. A* **2014,** *2*, 6688–6702. (e) Tomishige,

K.; Nakagawa, Y.; Tamura, M. Selective Hydrogenolysis and Hydrogenation Using Metal Catalysts Directly Modified with Metal Oxide Species. *Green Chem.* **2017,** *19*, 2876–2924. (f) Nakagawa, Y.; Tamura, M.; Tomishige, K. Perspective on Catalyst Development for Glycerol Reduction to C3 Chemicals with Molecular Hydrogen. *Res. Chem. Intermed.* **2018,** *44*, 3879–3903. (g) Falcone, D. D.; Hack, J. H.; Klyushin, A. Y.; Knop-Gericke, A.; Schlogl, R.; Davis, R. J. Evidence for the Bifunctional Nature of Pt-Re Catalysts for Selective Glycerol Hydrogenolysis. *ACS Catal.* **2015,** *5*, 5679–5695.

(6) (a) Arundhathi, R.; Mizugaki, T.; Mitsudome, T.; Jitsukawa, K.; Kaneda, K. Highly Selective Hydrogenolysis of Glycerol to 1,3-Propanediol over a Boehmite-Supported Platinum/Tungsten Catalyst. *ChemSusChem* **2013,** *6*, 1345–1347. (b) Zhu, S. H.; Zhu, Y. L.; Hao, S. L.; Zheng, H. Y.; Mo, T.; Li, Y. W. One-Step Hydrogenolysis of Glycerol to Biopropanols over Pt-$H_4SiW_{12}O_{40}/ZrO_2$ catalysts. *Green Chem.* **2012,** *14*, 2607–2616. (c) Zhou, W.; Luo, J.; Wang, Y.; Liu, J. F.; Zhao, Y. J.; Wang, S. P.; Ma, X. B. WO_x Domain Size, Acid Properties and Mechanistic Aspects of Glycerol Hydrogenolysis over Pt/WO_x/ZrO_2. *Appl. Catal. B* **2019,** *242*, 410–421. (d) Fan, Y. Q.; Cheng, S. J.; Wang, H.; Tian, J.; Xie, S. H.; Pei, Y.; Qiao, M. H.; Zong, B. N. Pt-WO_x on Monoclinic or Tetrahedral ZrO_2: Crystal Phase Effect of Zirconia on Glycerol Hydrogenolysis to 1,3-Propanediol. *Appl. Catal. B* **2017,** *217*, 331–341. (e) Fan, Y. Q.; Cheng, S. J.; Wang, H.; Ye, D. H.; Xie, S. H.; Pei, Y.; Hu, H. R.; Hua, W. M.; Li, Z. H.; Qiao, M. H.; Zong, B. N. Nanoparticulate Pt on Mesoporous SBA-15 Doped with Extremely Low Amount of W as a Highly Selective Catalyst for Glycerol Hydrogenolysis to 1,3-Propanediol. *Green Chem.* **2017,** *19*, 2174–2183.

(7) (a) Nakagawa, Y.; Shinmi, Y.; Koso, S.; Tomishige, K. Direct Hydrogenolysis of Glycerol into 1,3-Propanediol over Rhenium-Modified Iridium Catalyst. *J. Catal.* **2010,** *272*, 191–194. (b) Amada, Y.; Shinmi, Y.; Koso, S.; Kubota, T.; Nakagawa, Y.; Tomishige, K. Reaction Mechanism of the Glycerol Hydrogenolysis to 1,3-Propanediol over Ir-ReO_x/SiO_2 Catalyst. *Appl. Catal. B* **2011,** *105*, 117–127. (c) Nakagawa, Y.; Ning, X.; Amada, Y.; Tomishige, K. Solid Acid Co-Catalyst for the Hydrogenolysis of Glycerol to 1,3-Propanediol over Ir-ReO_x/SiO_2. *Appl. Catal. A* **2012,** *433*, 128–134. (d) Deng, C. H.; Duan, X. Z.; Zhou, J. H.; Zhou, X. G.; Yuan, W. K.; Scott, S. L. Ir-Re Alloy as a Highly Active Catalyst for the Hydrogenolysis of Glycerol to 1,3-Propanediol. *Catal. Sci. Technol.* **2015,** *5*, 1540–1547.

(8) Wang, J.; Zhao, X. C.; Lei, N.; Li, L.; Zhang, L. L.; Xu, S. T.; Miao, S.; Pan, X. L.; Wang, A. Q.;

Zhang, T. Hydrogenolysis of Glycerol to 1,3-Propanediol under Low Hydrogen Pressure over WO_x-Supported Single/Pseudo-Single Atom Pt Catalyst. *ChemSusChem* **2016,** *9*, 784–790.

(9) (a) Amada, Y.; Watanabe, H.; Tamura, M.; Nakagawa, Y.; Okumura, K.; Tomishige, K. Structure of ReO_x Clusters Attached on the Ir Metal Surface in Ir-ReO_x/SiO_2 for the Hydrogenolysis Reaction. *J. Phys. Chem. C* **2012,** *116*, 23503–23514. (b) Liu, L.; Kawakami, S.; Nakagawa, Y.; Tamura, M.; Tomishige, K. Highly Active Iridium–Rhenium Catalyst Condensed on Silica Support for Hydrogenolysis of Glycerol to 1, 3-Propanediol. *Appl. Catal. B* **2019,** *256*, 117775.

(10) Liu, S.; Zheng, W.; Fu, J.; Alexopoulos, K.; Saha, B.; Vlachos, D. G. Molybdenum Oxide-Modified Iridium Catalysts for Selective Production of Renewable Oils for Jet and Diesel Fuels and Lubricants. *ACS Catal.* **2019,** 7679–7689.

(11) (a) Nakagawa, Y.; Mori, K.; Chen, K.; Amada, Y.; Tamura, M.; Tomishige, K. Hydrogenolysis of C-O Bond over Re-Modified Ir Catalyst in Alkane Solvent. *Appl. Catal. A* **2013,** *468*, 418–425. (b) Chen, K.; Mori, K.; Watanabe, H.; Nakagawa, Y.; Tomishige, K. C-O Bond Hydrogenolysis of Cyclic Ethers with OH Groups over Rhenium-Modified Supported Iridium Catalysts. *J. Catal.* **2012,** *294*, 171–183. (c) Amada, Y.; Watanabe, H.; Hirai, Y.; Kajikawa, Y.; Nakagawa, Y.; Tomishige, K. Production of Biobutanediols by the Hydrogenolysis of Erythritol. *ChemSusChem* **2012,** *5*, 1991–1999. (d) Chen, K.; Tamura, M.; Yuan, Z.; Nakagawa, Y.; Tomishige, K. One-Pot Conversion of Sugar and Sugar Polyols to n-Alkanes without C-C Dissociation over the Ir-ReO_x/SiO_2 Catalyst Combined with H-ZSM-5. *ChemSusChem* **2013,** *6*, 613–621. (e) Liu, S.; Okuyama, Y.; Tamura, M.; Nakagawa, Y.; Imai, A.; Tomishige, K. Production of Renewable Hexanols from Mechanocatalytically Depolymerized Cellulose by Using Ir-ReO_x/SiO_2 catalyst. *ChemSusChem* **2015,** *8*, 628–635. (f) Tamura, M.; Tokonami, K.; Nakagawa, Y.; Tomishige, K. Selective Hydrogenation of Crotonaldehyde to Crotyl Alcohol over Metal Oxide Modified Ir Catalyst and Mechanistic Insight. *ACS Catal.* **2016,** *6*, 3600–3609. (g) Liu, S. B.; Dutta, S.; Zheng, W. Q.; Gould, N. S.; Cheng, Z. W.; Xu, B. J.; Saha, B.; Vlachos, D. G. Catalytic Hydrodeoxygenation of High Carbon Furylmethanes to Renewable Jet-Fuel Ranged Alkanes over a Rhenium-Modified Iridium Catalyst. *ChemSusChem* **2017,** *10*, 3225–3234. (h) Liu, S. B.; Simonetti, T.; Zheng, W. Q.; Saha, B. Selective Hydrodeoxygenation of Vegetable Oils and Waste Cooking Oils to Green Diesel Using a Silica-Supported Ir-ReO_x Bimetallic Catalyst. *ChemSusChem* **2018,** *11*, 1446–1454. (i) Liu, S. B.; Josephson, T. R.; Athaley, A.; Chen, Q. P.; Norton,

A.; Ierapetritou, M.; Siepmann, J. I.; Saha, B.; Vlachos, D. G. Renewable Lubricants with Tailored Molecular Architecture. *Sci. Adv.* **2019,** *5*, eaav5487. (j) Mascal, M.; Dutta, S.; Gandarias, I. Hydrodeoxygenation of the Angelica Lactone Dimer, a Cellulose-Based Feedstock: Simple, High-Yield Synthesis of Branched C_7-C_{10} Gasoline-like Hydrocarbons. *Angew. Chem. Int. Ed.* **2014,** *53*, 1854–1857. (k) Tomishige, K.; Tamura, M.; Nakagawa, Y. Role of Re Species and Acid Cocatalyst on Ir-ReO_x/SiO_2 in the C-O Hydrogenolysis of Biomass-Derived Substrates. *Chem. Rec.* **2014,** *14*, 1041–1054.

(12) (a) Mejia, C. H.; van Deelen, T. W.; de Jong, K. P. Activity Enhancement of Cobalt Catalysts by Tuning Metal-Support Interactions. *Nat. Commun.* **2018,** *9*, 1–8. (b) Zhao, E. W.; Zheng, H. B.; Ludden, K.; Xin, Y.; Hagelin-Weaver, H. E.; Bowers, C. R. Strong Metal-Support Interactions Enhance the Pairwise Selectivity of Parahydrogen Addition over Ir/TiO_2. *ACS Catal.* **2016,** *6*, 974–978. (c) Comotti, M.; Li, W. C.; Spliethoff, B.; Schuth, F. Support Effect in High Activity Gold Catalysts for CO Oxidation. *J. Am. Chem. Soc.* **2006,** *128*, 917-924. (d) Abad, A.; Concepcion, P.; Corma, A.; Garcia, H. A Collaborative Effect Between Gold and a Support Induces the Selective Oxidation of Alcohols. *Angew. Chem. Int. Ed.* **2005,** *44*, 4066–4069. (e) Li, S. W.; Xu, Y.; Chen, Y. F.; Li, W. Z.; Lin, L. L.; Li, M. Z.; Deng, Y. C.; Wang, X. P.; Ge, B. H.; Yang, C.; Yao, S. Y.; Xie, J. L.; Li, Y. W.; Liu, X.; Ma, D. Tuning the Selectivity of Catalytic Carbon Dioxide Hydrogenation over Iridium/Cerium Oxide Catalysts with a Strong Metal-Support Interaction. *Angew. Chem. Int. Ed.* **2017,** *56*, 10761–10765.

(13) Farmer, J. A.; Campbell, C. T. Ceria Maintains Smaller Metal Catalyst Particles by Strong Metal-Support Bonding. *Science* **2010,** *329*, 933–936.

(14) (a) Lykhach, Y.; Kozlov, S. M.; Skala, T.; Tovt, A.; Stetsovych, V.; Tsud, N.; Dvorak, F.; Johanek, V.; Neitzel, A.; Myslivecek, J.; Fabris, S.; Matolin, V.; Neyman, K. M.; Libuda, J. Counting Electrons on Supported Nanoparticles. *Nat. Mater.* **2016,** *15*, 284–288. (b) Liu, X. Y.; Liu, M. H.; Luo, Y. C.; Mou, C. Y.; Lin, S. D.; Cheng, H. K.; Chen, J. M.; Lee, J. F.; Lin, T. S. Strong Metal-Support Interactions between Gold Nanoparticles and ZnO Nanorods in CO Oxidation. *J. Am. Chem. Soc.* **2012,** *134*, 10251–10258. (c) Bruix, A.; Rodriguez, J. A.; Ramirez, P. J.; Senanayake, S. D.; Evans, J.; Park, J. B.; Stacchiola, D.; Liu, P.; Hrbek, J.; Illas, F. A New Type of Strong Metal-Support Interaction and the Production of H_2 through the Transformation of Water on Pt/CeO_2(111) and Pt/CeO_x/TiO_2(110)

Catalysts. *J. Am. Chem. Soc.* **2012,** *134*, 8968–8974. (d) He, J. Y.; Burt, S. P.; Ball, M.; Zhao, D. T.; Hermans, I.; Dumesic, J. A.; Huber, G. W. Synthesis of 1,6-Hexanediol from Cellulose Derived Tetrahydrofuran-Dimethanol with Pt-WO_x/TiO_2 Catalysts. *ACS Catal.* **2018,** *8*, 1427–1439.

(15) (a) Tauster, S. J.; Fung, S. C.; Garten, R. L. Strong Metal-Support Interractions. Group 8 Noble-Metals Supported on TiO_2. *J. Am. Chem. Soc.* **1978,** *100*, 170–175. (b) Matsubu, J. C.; Zhang, S. Y.; DeRita, L.; Marinkovic, N. S.; Chen, J. G. G.; Graham, G. W.; Pan, X. Q.; Christopher, P. Adsorbate-Mediated Strong Metal-Support Interactions in Oxide-Supported Rh Catalysts. *Nat. Chem.* **2017,** *9*, 120–127.

(16) Saavedra, J.; Doan, H. A.; Pursell, C. J.; Grabow, L. C.; Chandler, B. D. The Critical Role of Water at the Gold-Titania Interface in Catalytic CO Oxidation. *Science* **2014,** *345*, 1599–1602.

(17) (a) Akita, T.; Okumura, M.; Tanaka, K.; Tsubota, S.; Haruta, M. Analytical TEM observation of au and ir deposited on rutile TiO2. *J. Electron Microsc.* **2003,** *52*, 119–124. (b) Aranda-Perez, N.; Ruiz, M. P.; Echave, J.; Faria, J. Enhanced Activity and Stability of Ru-TiO_2 Rutile for Liquid Phase Ketonization. *Appl. Catal. A* **2017,** *531*, 106–118.

(18) (a) Liu, S.; Tang, N. F.; Shang, Q. H.; Wu, C. T.; Xu, G. L.; Cong, Y. Superior Performance of Iridium Supported on Rutile Titania for the Catalytic Decomposition of N_2O Propellants. *Chin. J. Catal.* **2018,** *39*, 1189–1193. (b) Bokhimi, X.; Zanella, R.; Angeles-Chavez, C. Rutile-Supported Ir, Au, and Ir-Au Catalysts for CO Oxidation. *J. Phys. Chem. C* **2010,** *114*, 14101–14109. (c) Fukutake, T.; Wada, K.; Liu, G. C.; Hosokawa, S.; Feng, Q. Striking Effects of a Titania Support on the Low-Temperature Activities of Ir Catalysts for the Dehydrogenative Synthesis of Benzimidazole and Indole. *Catal. Today* **2018,** *303*, 235–240.

(19) Gao, W.; Hood, Z. D.; Chi, M. Interfaces in Heterogeneous Catalysts: Advancing Mechanistic Understanding through Atomic-Scale Measurements. *Acc. Chem. Res.* **2017,** *50*, 787–795.

(20) (a) Huang, X.; Teschner, D.; Dimitrakopoulou, M.; Fedorov, A.; Frank, B.; Kraehnert, R.; Rosowski, F.; Kaiser, H.; Schunk, S.; Kuretschka, C.; Schlögl, R.; Willinger, M.-G.; Trunschke, A. Atomic-Scale Observation of the Metal–Promoter Interaction in Rh-Based Syngas-Upgrading Catalysts. *Angew. Chem. Int. Ed.* **2019,** *58*, 8709–8713. (b) Liu, Y.; Göeltl, F.; Ro, I.; Ball, M. R.; Sener, C.; Aragão, I. B.; Zanchet, D.; Huber, G. W.; Mavrikakis, M.; Dumesic, J. A. Synthesis Gas Conversion over Rh-Based Catalysts Promoted by Fe and Mn. *ACS Catal.* **2017,** *7*, 4550–4563.

(21) (a) Amada, Y.; Ota, N.; Tamura, M.; Nakagawa, Y.; Tomishige, K. Selective Hydrodeoxygenation of Cyclic Vicinal Diols to Cyclic Alcohols over Tungsten Oxide-Palladium Catalysts. *ChemSusChem* **2014,** *7*, 2185–2192. (b) Koso, S.; Watanabe, H.; Okumura, K.; Nakagawa, Y.; Tomishige, K. Comparative Study of Rh-MoO_x and Rh-ReO_x Supported on SiO_2 for the Hydrogenolysis of Ethers and Polyols. *Appl. Catal. B* **2012,** *111–112*, 27–37.

(22) (a) Jacobs, G.; Das, T. K.; Zhang, Y.; Li, J.; Racoillet, G.; Davis, B. H. Fischer–Tropsch Synthesis: Support, Loading, and Promoter Effects on the Reducibility of Cobalt Catalysts. *Appl. Catal. A* **2002,** *233*, 263–281. (b) Montes, M.; Getton, F. P.; Vong, M. S. W.; Sermon, P. A. Titania on Silica. A Comparison of Sol-Gel Routes and Traditional Methods. *J. Sol-Gel Sci. Technol.* **1997,** *8*, 131–137.

(23) Ishida, Y.; Ebashi, T.; Ito, S.; Kubota, T.; Kunimori, K.; Tomishige, K. Preferential CO Oxidation in a H_2-Rich Stream Promoted by ReO_x Species Attached to Pt Metal Particles. *Chem. Commun.* **2009,** 5308–5310.

(24) Tauster, S. J.; Fung, S. C.; Baker, R. T. K.; Horsley, J. A. Strong Interactions in Supported-Metal Catalysts. *Science* **1981,** *211*, 1121–1125.

(25) Xu, M.; He, S.; Chen, H.; Cui, G. Q.; Zheng, L. R.; Wang, B.; Wei, M. TiO_{2-x}-Modified Ni Nanocatalyst with Tunable Metal-Support Interaction for Water-Gas Shift Reaction. *ACS Catal.* **2017,** *7*, 7600–7609.

(26) Wan, X.; Zhang, Q.; Zhu, M.; Zhao, Y.; Liu, Y.; Zhou, C.; Yang, Y.; Cao, Y. Interface Synergy between IrO_x and H-ZSM-5 in Selective C–O Hydrogenolysis of Glycerol toward 1, 3-Propanediol. *J. Catal.* **2019,** *375*, 339–350.

(27) Tamura, M.; Yonezawa, D.; Oshino, T.; Nakagawa, Y.; Tomishige, K. In Situ Formed Fe Cation Modified Ir/MgO Catalyst for Selective Hydrogenation of Unsaturated Carbonyl Compounds. *ACS Catal.* **2017,** *7*, 5103–5111.

(28) Zhang, J.; Wang, H.; Wang, L.; Ali, S.; Wang, C.; Wang, L.; Meng, X.; Li, B.; Su, D. S.; Xiao, F.-S. Wet-Chemistry Strong Metal–Support Interactions in Titania-Supported Au Catalysts. *J. Am. Chem. Soc.* **2019,** *141*, 2975–2983.

(29) Ly, B. K.; Tapin, B.; Aouine, M.; Delichere, P.; Epron, F.; Pinel, C.; Especel, C.; Besson, M. Insights into the Oxidation State and Location of Rhenium in Re-Pd/TiO_2 Catalysts for Aqueous-Phase Selective Hydrogenation of Succinic Acid to 1,4-Butanediol as a Function of Palladium and Rhenium

Deposition Methods. *ChemCatChem* **2015,** *7*, 2161–2178.

(30) Freakley, S. J.; Ruiz-Esquius, J.; Morgan, D. J. The X-ray Photoelectron Spectra of Ir, IrO_2 and $IrCl_3$ Revisited. *Surf. Interface Anal.* **2017,** *49*, 794–799.

(31) Takeda, Y.; Tamura, M.; Nakagawa, Y.; Okumura, K.; Tomishige, K. Characterization of Re-Pd/SiO_2 Catalyst for Hydrogenation of Stearic Acid. *ACS Catal.* **2015,** *5*, 7034–7047.

(32) Beamson, G.; Papworth, A. J.; Philipps, C.; Smith, A. M.; Whyman, R. Selective Hydrogenation of Amides Using Bimetallic Ru/Re and Rh/Re Catalysts. *J. Catal.* **2011,** *278*, 228–238.

(33) (a) Said, A.; Da Silva Perez, D.; Perret, N.; Pinel, C.; Besson, M. Selective C−O Hydrogenolysis of Erythritol over Supported Rh-ReO_x Catalysts in the Aqueous Phase. *ChemCatChem* **2017,** *9*, 2768–2783. (b) Sadier, A.; Perret, N.; Da Silva Perez, D.; Besson, M.; Pinel, C. Effect of Carbon Chain Length on Catalytic C-O Bond Cleavage of Polyols over Rh-ReO_x/ZrO_2 in Aqueous Phase. *Appl. Catal. A* **2019,** *586*, 117213.

(34) Nakagawa, Y.; Takada, K.; Tamura, M.; Tomishige, K. Total Hydrogenation of Furfural and 5-Hydroxymethylfurfural over Supported Pd-Ir Alloy Catalyst. *ACS Catal.* **2014,** *4*, 2718–2726.

(35) (a) Rygh, L. E. S.; Nielsen, C. J. Infrared Study of CO Adsorbed on a Co/Re/Gamma Al_2O_3-Based Fischer-Tropsch Catalyst. *J. Catal.* **2000,** *194*, 401–409. (b) Sojymosi, F.; Zakar, T. S. FT-IR Study on the Interaction of CO_2 with H_2 and Hydrocarbons over Supported Re. *J. Mol. Catal. A* **2005,** *235*, 260–266.

(36) (a) Gomez-Cortes, A.; Diaz, G.; Zanella, R.; Ramirez, H.; Santiago, P.; Saniger, J. M. Au-Ir/TiO_2 Prepared by Deposition Precipitation with Urea: Improved Activity and Stability in CO Oxidation. *J. Phys. Chem. C* **2009,** *113*, 9710–9720. (b) Song, Y.-J.; López-De Jesús, Y. M.; Fanson, P. T.; Williams, C. T. Preparation and Characterization of Dendrimer-Derived Bimetallic Ir–Au/Al_2O_3 Catalysts for CO Oxidation. *J. Phys. Chem. C* **2013,** *117*, 10999–11007. (c) Song, Y.-J.; Jesús, Y. M. L.-D.; Fanson, P. T.; Williams, C. T. Kinetic Evaluation of Direct NO Decomposition and NO–CO Reaction over Dendrimer-Derived Bimetallic Ir–Au/Al_2O_3 Catalysts. *Appl. Catal. B* **2014,** *154–155*, 62–72. (d) Song, Y.-J.; Monnier, J. R.; Fanson, P. T.; Williams, C. T. Bimetallic Ag–Ir/Al_2O_3 Catalysts Prepared by Electroless Deposition: Characterization and Kinetic Evaluation. *J. Catal.* **2014,** *315*, 59–66.

Figure caption

Figure 1. Glycerol hydrogenolysis over Ir-ReO_x catalysts (Ir: 4 wt%, Re/Ir = 0.25, nominal) on various supports (A) and effect of Ir loading amount (Re/Ir = 0.25, nominal) on glycerol hydrogenolysis (B). Reaction conditions: catalyst amount varied to keep total nominal Ir amount of 31 μmol, glycerol = 4 g (43 mmol), H_2O = 2 g, $P(H_2)$ = 8 MPa, T = 393 K, t = 8 h (A) or 4 h (B). Reduction conditions: H_2 flow at 573 K (G, 573).

a: $Ir(NO_3)_4$ as Ir precursor.

b: Ir-ReO_x/SiO_2 (4 wt% Ir, Re/Ir = 1, nominal), reduced in water at 473 K (L, 473); data from Ref. 9b.

c: Ir-ReO_x/SiO_2 (20 wt% Ir, Re/Ir = 1, nominal), reduced in water at 473 K (L, 473); data from Ref. 9b.

Figure 2. Kinetics study of glycerol hydrogenolysis over 4 wt%-Ir Ir-ReO_x/Rutile (Re/Ir = 0.24*) catalyst. (A) Effect of hydrogen pressure (v_g: conversion rate of glycerol). (B) Effect of glycerol concentration. Details of reaction conditions and results are summarized in Tables S3 and S4. Reduction conditions: H_2 flow at 573 K (G, 573).

Figure 3. TPR profiles of 4 wt%-Ir Ir-ReO_x/Rutile with different ratio of Re to Ir (actual ratio* (nominal ratio)), (a) 0.7 wt% ReO_x/Rutile, (b) 4 wt% Ir/Rutile, (c) Re/Ir = 0.08* (0.063) (d) 0.12* (0.13), (e) 0.24* (0.25), (f) 0.25* (0.5), (g) 0.30* (1), (h) 0.27* (0.25), precursor of $Ir(NO_3)_4$, (actual ratio). Y-axis was normalized by the weight of catalysts. Conditions: H_2/Ar (5% v/v, 30 cm^3 min^{-1}) at heating rate of 10 K min^{-1}. Dotted line represents the baseline for H_2 consumption amount calculation.

Figure 4. TEM images of catalysts: (A) Ir/Anatase, (B) Ir/Rutile and (C) Ir/P25, Ir: 4 wt%; (D) Ir-ReO_x/Anatase, (E) Ir-ReO_x/Rutile, (F) Ir-ReO_x/P25, Ir: 4 wt%, Re/Ir = 0.25. Catalysts were pre-reduced by H_2 at 573 K for 1 h before measurement.

Figure 5. Results of XPS for Ir 4f fitting results of (A) 4 wt% Ir/Rutile, (B) 4 wt%-Ir Ir-ReO_x/Rutile (Re/Ir = 0.24*), (C) 4 wt%-Ir Ir-ReO_x/Rutile (Re/Ir = 0.30*), (D) 4 wt%-Ir Ir-ReO_x/Rutile (Re/Ir = 0.24*) after passivation by 1% O_2/He, and (E), (F), and (G) of corresponding Re 4f fitting results. All the samples were pre-reduced by H_2 flow (100% H_2, 30 mL min^{-1}) at 573 K for 1 h (G, 573). Analysis result is shown in Table 7.

Figure 6. DRIFT spectra of CO adsorbed on the Ir-ReO_x/Rutile catalysts after reduction at 573 K. (A) The raw profiles of spectra, (B) Curve fitting results of spectra (A) at range of 2030-2110 cm^{-1} by Gaussian function and analysis results are shown in Table S7. Y-axis is normalized by corresponding D_{CO}.

(a) 4 wt% Ir/Rutile, (b) 4 wt%-Ir Ir-ReO_x/Rutile (Re/Ir = 0.24*), (c) 4 wt%-Ir Ir-ReO_x/Rutile (Re/Ir = 0.30*), (d) 2 wt%-Ir Ir-ReO_x/Rutile (Re/Ir = 0.32*), (e) 6 wt%-Ir Ir-ReO_x/Rutile (Re/Ir = 0.18*), (f) 8 wt%-Ir Ir-ReO_x/Rutile (Re/Ir = 0.15*).

Figure 7. Relationship between catalytic performance and (A) average CN of Re-Re (or -Ir) (black curve) and the density of surface Ir^0 surface on Ir-ReO_x/Rutile catalysts with different Ir loading amount (red curve), and (B) surface Re/Ir ratio (Table 7) on 4 wt%-Ir Ir-ReO_x/Rutile catalysts. Reaction conditions: Detailed results are shown in Table S8.

Figure 8. Proposed catalyst structure of Ir-ReO_x/Rutile catalyst after reduction at 573 K.

Table 1 Effect of additive amount of Re on the glycerol hydrogenolysis over 4 wt% Ir-ReO_x/Rutile and related catalysts

Catalyst	Re/Ir ratio		Conv.	Selectivity / %				
	nominal	actual[c]	/ %	1,3-PrD	1,2-PrD	1-PrOH	2-PrOH	Others
Ir/Rutile	-	-	<0.5	-	-	-	-	-
Ir-ReO_x/Rutile	0.063	0.08*	11	73	1	19	5	2
	0.13	0.12*	21	70	2	20	5	3
	0.25	0.24*	35	67	2	25	5	1
	0.5	0.25*	45	60	2	32	5	1
	1	0.30*	52	57	2	34	5	2
ReO_x/Rutile[a]	-	-	<0.1	-	-	-	-	-
Ir-ReO_x/Rutile + H_2SO_4[b]	0.25	0.24	43	64	2	28	5	1

Reaction conditions: catalyst amount = 150 mg (Ir: 31 μmol), glycerol = 4 g (43 mmol), H_2O = 2 g, $P(H_2)$ = 8 MPa, T = 393 K, t = 4 h. Reduction conditions: H_2 flow at 573 K (G, 573).

[a]Re loading amount of 0.9 wt%. [b]H^+/Ir = 1, molar ratio. [c]Determined from XRF analysis.

Table 2 Accurate loading amount of Ir and Re on TiO_2 support determined by XRF

Entry	Catalyst	Re/Ir ratio (nominal)	Composition (wt%)		Re/Ir ratio (actual)
			Ir	Re	
1	4 wt% Ir/Rutile	-	4.0	-	0
2	ReO_x/Rutile	(0.9 wt%)[a]	-	0.7	-
3	4 wt%-Ir Ir-ReO_x/Rutile	0.063	4.0	0.3	0.08*
4		0.13	4.2	0.5	0.12*
5		0.25	3.9	0.9	0.24*
6		0.5	4.1	1.0	0.25*
7		1	4.2	1.2	0.30*
8	4 wt%-Ir Ir-ReO_x/Rutile[b]	0.25	4.4	1.2	0.27*
9	2 wt%-Ir Ir-ReO_x/Rutile	0.25	1.8	0.6	0.32*
10	6 wt%-Ir Ir-ReO_x/Rutile	0.25	6.0	1.1	0.18*
11	8 wt%-Ir Ir-ReO_x/Rutile	0.25	8.6	1.3	0.15*
12	4 wt% Ir/Anatase	-	4.0	-	0
13	4 wt%-Ir Ir-ReO_x/Anatase	0.25	3.7	0.6	0.16*
14	4 wt% Ir/P25	-	3.9	-	0
15	4 wt%-Ir Ir-ReO_x/P25	0.25	3.9	1.2	0.30*

[a]Loading amount of Re. [b]Precursor of $Ir(NO_3)_4$.

Table 3 Glycerol hydrogenolysis over 4 wt%-Ir Ir-ReO_x/TiO_2 catalysts reduced at different conditions

Entry	Catalyst	Reduction condition	Conv. / %	Selectivity / %				
				1,3-PrD	1,2-PrD	1-PrOH	2-PrOH	Others
1	Ir-ReO_x/Rutile,	(L, 473)	24	71	4	18	6	1
2	Re/Ir = 0.24* (0.25)	(G, 473)	26	69	4	20	6	1
3		(G, 573)	35	67	2	25	5	1
4		(G, 673)	23	69	4	20	6	1
5		(G, 773)	13	69	10	14	7	< 1
6[a]		(G, 573)	22	67	4	23	5	1
7	Ir-ReO_x/Rutile,	(L, 473)	31	72	5	15	7	1
8	Re/Ir = 0.30* (1)	(G, 473)	46	59	3	31	6	1
9		(G, 573)	52	57	2	34	5	2
10		(G, 673)	36	61	4	28	6	1
11		(G, 773)	17	65	10	17	7	1
12	Ir-ReO_x/Anatase,	(L, 473)	2	48	31	8	12	1
13	Re/Ir = 0.16* (0.25)	(G, 473)	3	45	36	8	9	2
14		(G, 573)	<0.5	-	-	-	-	-
15	Ir-ReO_x/P25,	(L, 473)	6	71	8	12	8	1
16	Re/Ir = 0.30* (0.25)	(G, 473)	9	69	6	16	7	2
17		(G, 573)	11	72	6	16	5	1
18		(G, 673)	7	69	8	15	7	1
19		(G, 773)	7	71	8	13	7	1

Reaction conditions: catalyst amount = 150 mg, glycerol = 4 g, H_2O = 2 g, $P(H_2)$ = 8 MPa, T = 393 K, t = 4 h. Reduction conditions: 30 cm^3 min^{-1} H_2 at desired temperature for 1 h or P H_2 = 8 MPa at 473 K for 1 h (L, 473).
[a]Catalyst (G, 573) was passivated by 1 % O_2/He for 15 min at ambient temperature.

Table 4 Time course of glycerol hydrogenolysis over 4 wt%-Ir Ir-ReO_x/Rutile

t / h	Conv. / %	Selectivity / %					1,3-PrD yield / %	$P_{1,3\text{-PrD}}$ / g g_{Ir}^{-1} h^{-1}
		1,3-PrD	1,2-PrD	1-PrOH	2-PrOH	Others		
0	<1	-	-	-	-	-	-	-
1	12	73	1	19	4	3	9	-
2	26	71	2	22	4	1	18	52
4	35	67	2	25	5	1	24	-
8	59	58	1	33	6	2	34	-
12	69	52	2	38	6	2	36	17
16	80	45	1	44	7	3	36	-

Reaction conditions: catalyst = 150 mg (Ir: 31 μmol, Re/Ir = 0.24*), glycerol = 4 g (43 mmol), H_2O = 2 g, $P(H_2)$ = 8 MPa, T = 393 K. Reduction conditions: H_2 flow at 573 K (G, 573).

Table 5 Summary of characterization results of Ir-ReO_x/Rutile after reduction at 573 K

Entry	Catalyst	Re/Ir ratio (nominal)	TEM	Valence of Ir		Valence of Re		D_{CO} / %	Coverage / %[f]	$P_{1,3\text{-PrD}}$ / g g_{Ir}^{-1} h^{-1}
			d / nm[a]	XPS[b]	XANES[c]	XPS[d]	XANES[e]			
1	4 wt% Ir/Rutile	0	2.6	1.1	1.0	-	-	20	-	0.1
2	4 wt%-Ir Ir-ReO_x/Rutile	0.08* (0.063)	-	-	0.4	-	3.0	19	-	9
3	4 wt%-Ir Ir-ReO_x/Rutile	0.12* (0.13)	-	-	0.4	-	2.6	24	-	21
4	4 wt%-Ir Ir-ReO_x/Rutile	0.24* (0.25)	1.9	0.7	0.5	3.2	3.1	33	62	52
5	4 wt%-Ir Ir-ReO_x/Rutile	0.25* (0.5)		-	0.4	-	2.7	34	-	67
6	4 wt%-Ir Ir-ReO_x/Rutile	0.30* (1)	1.8	0.7	0.5	3.2	2.7	34	62	94
7	2 wt%-Ir Ir-ReO_x/Rutile	0.32* (0.25)	1.6	-	0.5	-	3.0	46	63	18
8	6 wt%-Ir Ir-ReO_x/Rutile	0.18* (0.25)	2.6	-	0.3	-	2.7	21	64	56
9	8 wt%-Ir Ir-ReO_x/Rutile	0.15* (0.25)	3.0	-	0.4	-	2.8	16	67	45

[a]The average particle size determined by TEM.

[b]The average valence of Ir (XPS) = 0 × Ir^0 surface ratio + 3 × Ir^{3+} surface ratio + 4 × Ir^{4+} surface ratio.

[c]The average valence of Ir (XANES) = 4 × $CN_{Ir\text{-}O}$/6, Ref. 9a.

[d]The average valence of Re (XPS) = 3 × Re^{3+} surface ratio + 4 × Re^{4+} surface ratio.

[e]The average valence of Re (XANES) was determined by white line intensity calibrated by standard references.

[f]The surface coverage of ReO_x on Ir metal = (1-D_{CO} × Ir^0 ratio (determined from CO FT-IR) / (1.1/d_{TEM})) × 100%.

Table 6 Reusability of 4 wt%-Ir Ir-ReO_x/Rutile

Glycerol amount / g	H_2O amount / g	Catalyst amount / mg	Usage times	Conv. / %	Selectivity / %					Conversion rate (v_g) / mmol·g-Cat^{-1} h^{-1}
					1,3-PrD	1,2-PrD	1-PrOH	2-PrOH	Others	
1.0	19.0	150	1	27	64	5	20	9	2	19.3
0.9	17.1	(135)[a]	2	26	63	5	21	9	2	(19.3)
0.8	15.2	(121)[a]	3	26	63	6	20	9	2	(19.6)
0.7	13.3	110	4	25	64	6	19	10	1	18.6

Reaction conditions: $P(H_2) = 8$ MPa, $T = 393$ K, $t = 1$ h. The initial amount of glycerol and H_2O (pre-degassed) was 1 g and 19 g, respectively. Catalyst of 4 wt%-Ir Ir-ReO_x/Rutile (Re/Ir = 0.24*) was pre-reduced by H_2 flow at 573 K for 1 h (G, 573).

[a]Estimated amount from the final catalyst amount.

Table 7 Results of XPS analysis over Ir/Rutile and Ir-ReO_x/Rutile after gas-phase reduction or passivation

Catalyst	Re/Ir ratio (nominal)	Ir^0 B.E.[a] / eV	Area ratio/ %	Ir^{3+} B.E.[a] / eV	Area ratio/ %	Ir^{4+} B.E.[a] / eV	Area ratio/ %	Re^{3+} B.E.[b] / eV	Area ratio/ %	Re^{4+} B.E.[b] / eV	Area ratio/ %	Re^{7+} B.E.[b] / eV	Area ratio/ %	$Re_{s,\ total}/Ir_{s,\ total}$
Ir (G,573)	-	60.6	68	61.7	21	62.7	11	-	-	-	-	-	-	-
Ir-ReO_x (G,573)	0.24* (0.25)	61.1	78	62.2	15	63.2	7	41.7	80	42.5	20	-	-	0.16
Ir-ReO_x (G,573)	0.30* (1)	61.1	80	62.2	13	63.2	7	41.7	78	42.5	22	-	-	0.25
Ir-ReO_x (G,573)[c]	0.24* (0.25)	61.0	74	62.1	17	63.0	9	41.2	39	42.0	10	45.8	51	0.16

[a]B.E.: binding energy for Ir $4f_{7/2}$. [b]B.E.: binding energy for Re $4f_{7/2}$. [c]Ir-ReO_x/Rutile (G, 573) after passivation by 1% O_2/He for 15 min at ambient temperature.

Table 8 Curve fitting results of Ir L_3-edge EXAFS of 4 wt% Ir/Rutile and Ir-ReO_x/Rutile after reduction or reaction

Entry	Catalyst	Shells	CN[a]	R / 10^{-1} nm[b]	σ / 10^{-1} nm[c]	ΔE_0 / eV[d]	R_f / %[e]
1	Ir/Rutile (G, 573)	Ir-O	1.5	2.12	0.070	10.3	0.4
		Ir-Ir	8.2	2.74	0.062	-1.4	
2	Ir/Rutile (G, 573) after reaction	Ir-O	1.2	2.11	0.065	3.3	2.8
		Ir-Ir	8.6	2.76	0.061	1.4	
3	4 wt%-Ir Ir-ReO_x/Rutile (G, 573) (Re/Ir = 0.24*)	Ir-O	0.7	2.03	0.060	-9.3	1.1
		Ir-Ir (or -Re)	8.7	2.74	0.060	-1.7	
4	4 wt%-Ir Ir-ReO_x/Rutile (G, 573) (Re/Ir = 0.24*) after reaction	Ir-O	0.6	2.03	0.060	1.8	2.4
		Ir-Ir (or -Re)	8.6	2.75	0.060	-3.4	
5	4 wt%-Ir Ir-ReO_x/Rutile (G, 573) (Re/Ir = 0.30*)	Ir-O	0.7	2.03	0.060	-5.6	2.6
		Ir-Ir (or -Re)	9.0	2.75	0.067	-0.6	
6	4 wt%-Ir Ir-ReO_x/Rutile (G, 573) (Re/Ir = 0.30*) after reaction	Ir-O	0.7	2.03	0.060	-4.6	1.5
		Ir-Ir (or -Re)	8.9	2.75	0.064	-2.3	
7	4 wt%-Ir Ir-ReO_x/Rutile (G, 573) (Re/Ir = 0.08*)	Ir-O	0.6	2.03	0.066	-1.1	2.0
		Ir-Ir (or -Re)	8.7	2.74	0.062	-2.1	
8	4 wt%-Ir Ir-ReO_x/Rutile (G, 573) (Re/Ir = 0.12*)	Ir-O	0.6	2.03	0.071	-1.2	0.4
		Ir-Ir (or -Re)	9.0	2.74	0.060	-1.4	
9	4 wt%-Ir Ir-ReO_x/Rutile (G, 573) (Re/Ir = 0.25*)	Ir-O	0.6	2.03	0.070	-0.3	1.0
		Ir-Ir (or -Re)	8.9	2.74	0.065	-4.9	
10	2 wt%-Ir Ir-ReO_x/Rutile (G, 573) (Re/Ir = 0.32*)	Ir-O	0.8	2.03	0.070	-6.0	2.6
		Ir-Ir (or -Re)	7.8	2.74	0.065	-1.3	
11	6 wt%-Ir Ir-ReO_x/Rutile (G, 573) (Re/Ir = 0.18*)	Ir-O	0.5	2.03	0.070	-10.4	1.1
		Ir-Ir (or -Re)	9.7	2.74	0.063	-2.4	
12	8 wt%-Ir Ir-ReO_x/Rutile (G, 573) (Re/Ir = 0.15*)	Ir-O	0.6	2.03	0.070	-4.8	0.8
		Ir-Ir (or -Re)	10.1	2.74	0.066	-2.1	
13	4 wt%-Ir Ir-ReO_x/SiO_2 (L, 473) (Re/Ir = 0.83*) after reaction[f]	Ir-Ir	10.5	2.76	0.066	-1.1	0.9
14	Ir powder	Ir-Ir	12	2.76	0.060	0	-
15	IrO_2	Ir-O	6	1.98	0.060	0	-

[a]Coordination number. [b]Bond distance. [c]Debye-Waller factor. [d]Difference in the origin of photoelectron energy between the reference and the sample. [e]Residual factor. Fourier filtering range: 0.156-0.325 nm. [f]Ir: 4 wt%, Re/Ir = 0.83*, Ref. 7b.

Table 9 Curve fitting results of Re L_3-edge EXAFS of Ir-ReO_x/Rutile after reduction or reaction

Entry	Catalyst	Shells	CN[a]	R / 10^{-1} nm[b]	σ / 10^{-1} nm[c]	ΔE_0 / eV[d]	R_f / %[e]
1	4 wt%-Ir Ir-ReO_x/Rutile (G, 573) (Re/Ir = 0.24*)	Re-O	0.6	2.12	0.079	9.9	1.9
		Re-Re (or -Ir)	8.6	2.63	0.066	-9.6	
2	4 wt%-Ir Ir-ReO_x/Rutile (G, 573) after reaction (Re/Ir = 0.24*)	Re-O	0.6	2.11	0.078	9.9	2.9
		Re-Re (or -Ir)	8.8	2.64	0.065	-8.7	
3	4 wt%-Ir Ir-ReO_x/Rutile (G, 573) (Re/Ir = 0.30*)	Re-O	0.5	2.12	0.079	9.9	1.5
		Re-Re (or -Ir)	8.9	2.64	0.065	-8.1	
4	4 wt%-Ir Ir-ReO_x/Rutile (G, 573) after reaction (Re/Ir = 0.30*)	Re-O	0.5	2.12	0.060	10.1	1.2
		Re-Re (or -Ir)	8.6	2.64	0.066	-8.4	
5	4 wt%-Ir Ir-ReO_x/Rutile (G, 573) (Re/Ir = 0.08*)	Re-O	0.7	2.11	0.079	10.8	3.7
		Re-Re (or -Ir)	8.4	2.63	0.060	-8.9	
6	4 wt%-Ir Ir-ReO_x/Rutile (G, 573) (Re/Ir = 0.12*)	Re-O	0.6	2.12	0.078	9.9	1.4
		Re-Re (or -Ir)	8.5	2.63	0.063	-7.1	
7	4 wt%-Ir Ir-ReO_x/Rutile (G, 573) (Re/Ir = 0.25*)	Re-O	0.6	2.12	0.078	9.9	0.3
		Re-Re (or -Ir)	8.6	2.64	0.065	-6.3	
8	2 wt%-Ir Ir-ReO_x/Rutile (G, 573) (Re/Ir = 0.32*)	Re-O	1.1	2.12	0.077	10.2	1.6
		Re-Re (or -Ir)	5.9	2.64	0.064	-6.4	
9	6 wt%-Ir Ir-ReO_x/Rutile (G, 573) (Re/Ir = 0.18*)	Re-O	0.5	2.12	0.079	5.2	1.8
		Re-Re (or -Ir)	9.4	2.64	0.064	-6.9	
10	8 wt%-Ir Ir-ReO_x/Rutile (G, 573) (Re/Ir = 0.15*)	Re-O	0.6	2.12	0.079	10.2	1.6
		Re-Re (or -Ir)	10.4	2.64	0.060	-7.2	
11	4 wt%-Ir Ir-ReO_x/SiO_2 (L, 473) (Re/Ir = 0.83*) after reaction[f]	Re-O	1.4	2.02	0.074	-0.1	2.0
		Re-Re (or -Ir)	6.2	2.68	0.076	8.7	
12	Re powder	Re-Re	12	2.74	0.060	0	-

[a]Coordination number. [b]Bond distance. [c]Debye-Waller factor. [d]Difference in the origin of photoelectron energy between the reference and the sample. [e]Residual factor. Fourier filtering range: 0.156-0.325 nm. [f]Ir: 4 wt%, Re/Ir = 0.83*, Ref. 7b.

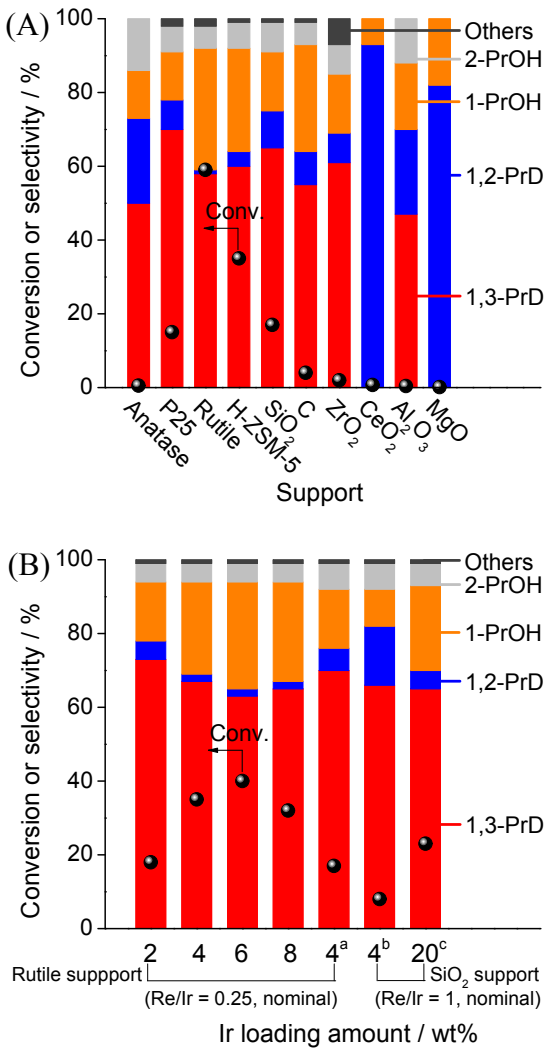

Figure 1. Glycerol hydrogenolysis over Ir-ReO_x catalysts (Ir: 4 wt%, Re/Ir = 0.25, nominal) on various supports (A) and effect of Ir loading amount (Re/Ir = 0.25, nominal) on glycerol hydrogenolysis (B). Reaction conditions: catalyst amount varied to keep total nominal Ir amount of 31 μmol, glycerol = 4 g (43 mmol), H_2O = 2 g, $P(H_2)$ = 8 MPa, T = 393 K, t = 8 h (A) or 4 h (B). Reduction conditions: H_2 flow at 573 K (G, 573).

a: $Ir(NO_3)_4$ as Ir precursor.

b: Ir-ReO_x/SiO_2 (4 wt% Ir, Re/Ir = 1, nominal), reduced in water at 473 K (L, 473); data from Ref. 9b.

c: Ir-ReO_x/SiO_2 (20 wt% Ir, Re/Ir = 1, nominal), reduced in water at 473 K (L, 473); data from Ref. 9b.

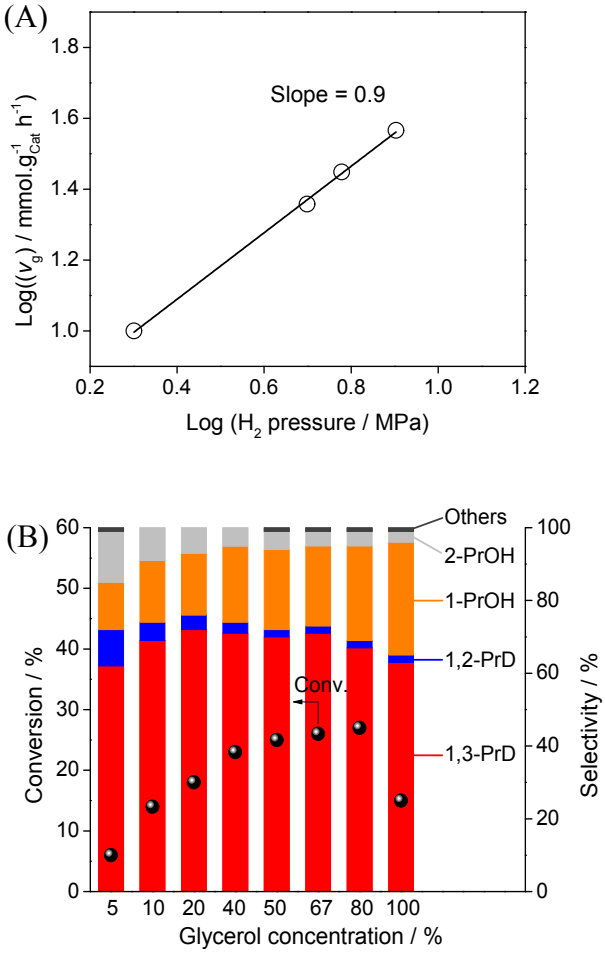

Figure 2. Kinetics study of glycerol hydrogenolysis over 4 wt%-Ir Ir-ReO_x/Rutile (Re/Ir = 0.24*) catalyst. (A) Effect of hydrogen pressure (v_g: conversion rate of glycerol). (B) Effect of glycerol concentration. Details of reaction conditions and results are summarized in Tables S3 and S4. Reduction conditions: H_2 flow at 573 K (G, 573).

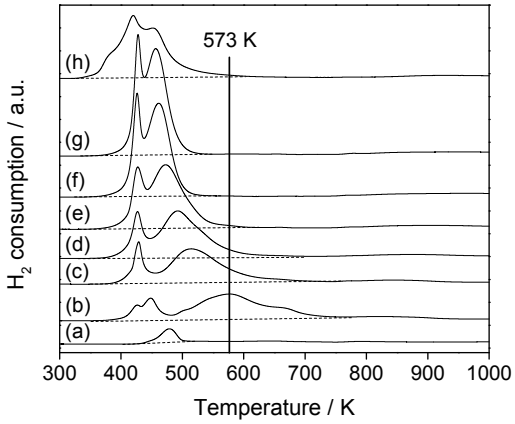

Figure 3. TPR profiles of 4 wt%-Ir Ir-ReO_x/Rutile with different ratio of Re to Ir (actual ratio* (nominal ratio)), (a) 0.7 wt% ReO_x/Rutile, (b) 4 wt% Ir/Rutile, (c) Re/Ir = 0.08* (0.063) (d) 0.12* (0.13), (e) 0.24* (0.25), (f) 0.25* (0.5), (g) 0.30* (1), (h) 0.27* (0.25), precursor of $Ir(NO_3)_4$, (actual ratio). Y-axis was normalized by the weight of catalysts. Conditions: H_2/Ar (5% v/v, 30 cm^3 min^{-1}) at heating rate of 10 K min^{-1}. Dotted line represents the baseline for H_2 consumption amount calculation.

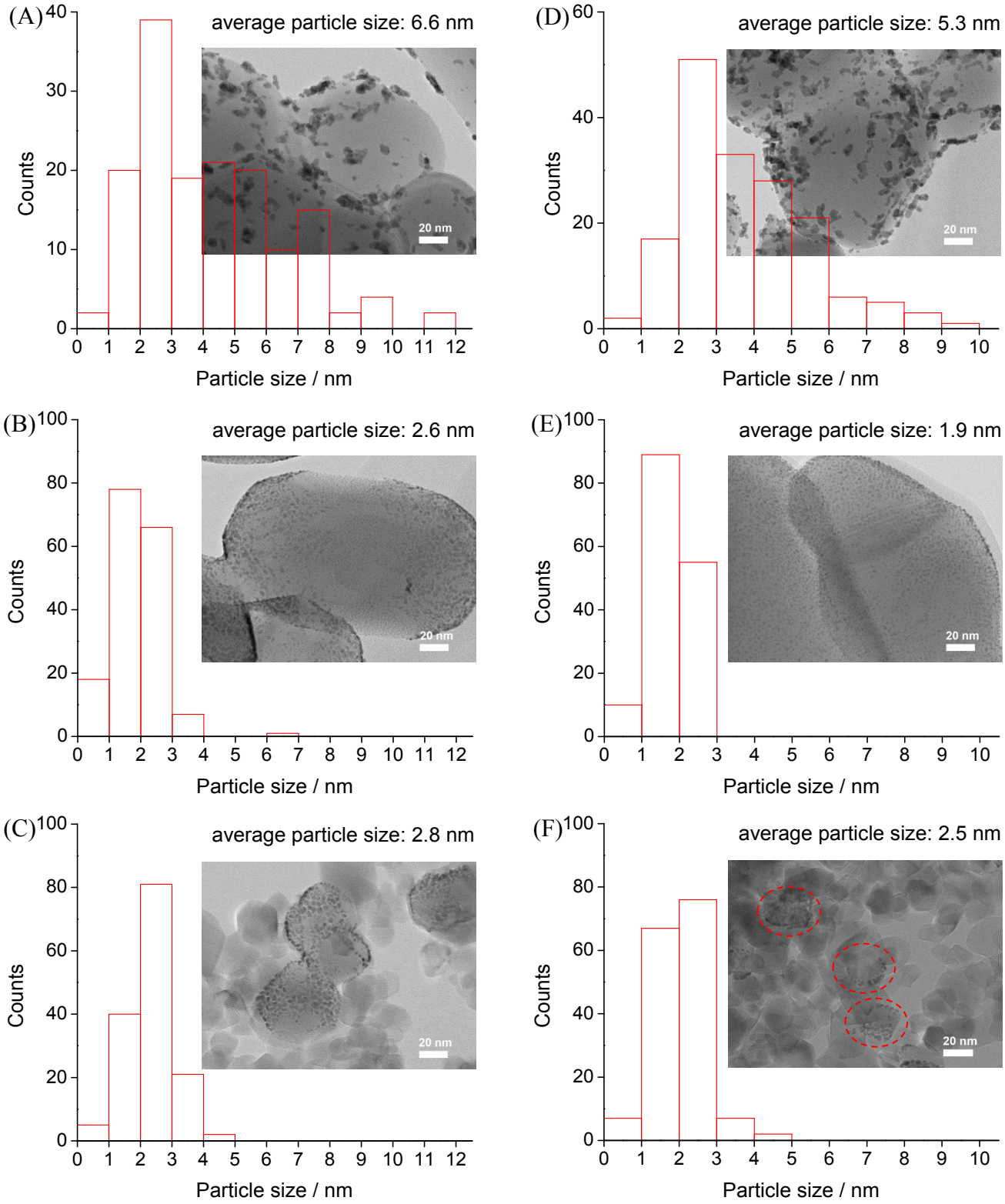

Figure 4. TEM images of catalysts: (A) Ir/Anatase, (B) Ir/Rutile and (C) Ir/P25, Ir: 4 wt%; (D) Ir-ReO_x/Anatase, (E) Ir-ReO_x/Rutile, (F) Ir-ReO_x/P25, Ir: 4 wt%, Re/Ir = 0.25. Catalysts were pre-reduced by H_2 at 573 K for 1 h before measurement.

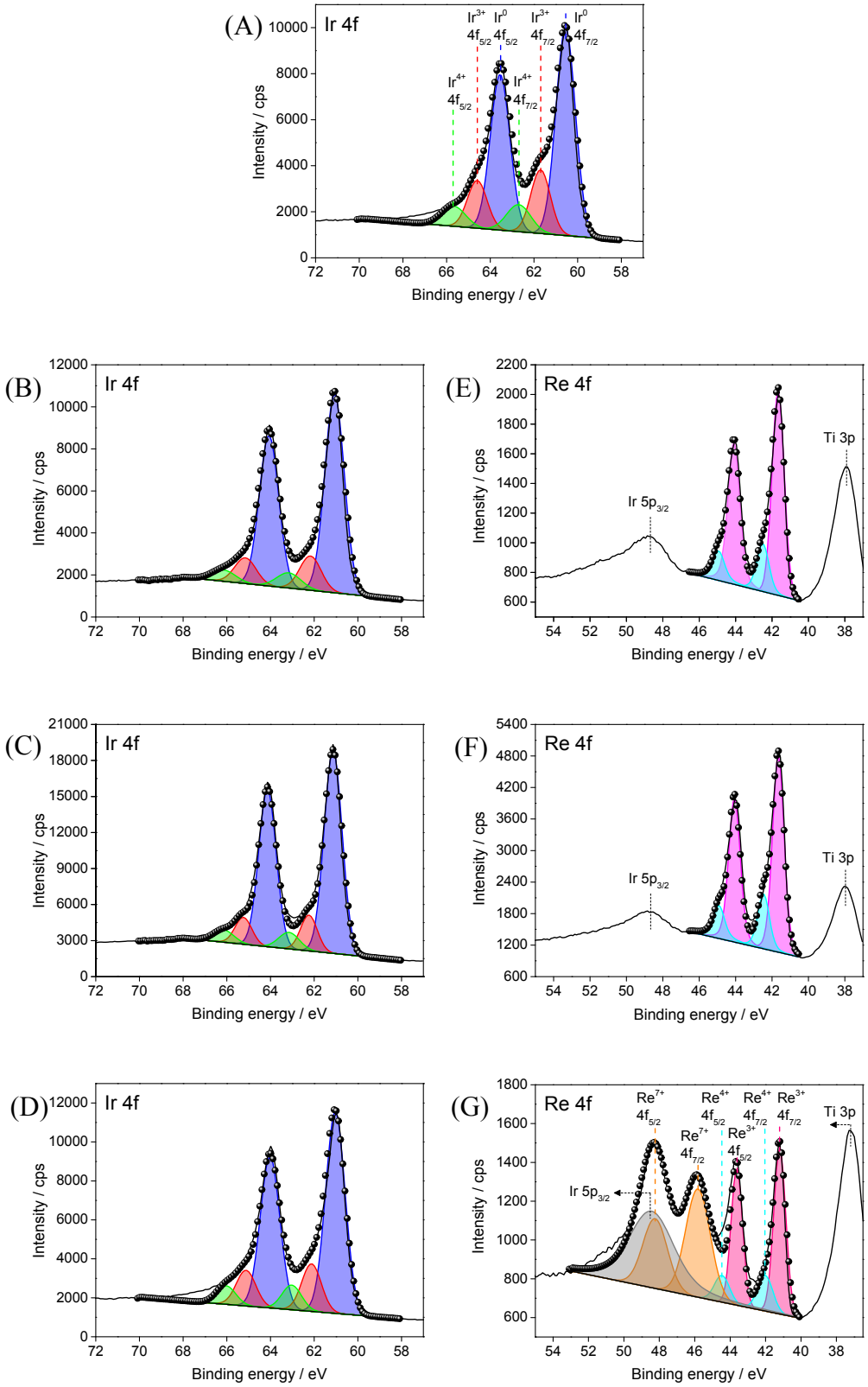

Figure 5. Results of XPS for Ir 4f fitting results of (A) 4 wt% Ir/Rutile, (B) 4 wt%-Ir Ir-ReO_x/Rutile (Re/Ir = 0.24*), (C) 4 wt%-Ir Ir-ReO_x/Rutile (Re/Ir = 0.30*), (D) 4 wt%-Ir Ir-ReO_x/Rutile (Re/Ir = 0.24*) after passivation by 1% O_2/He, and (E), (F), and (G) of corresponding Re 4f fitting results. All the samples were pre-reduced by H_2 flow (100% H_2, 30 mL min^{-1}) at 573 K for 1 h (G, 573). Analysis result is shown in Table 7.

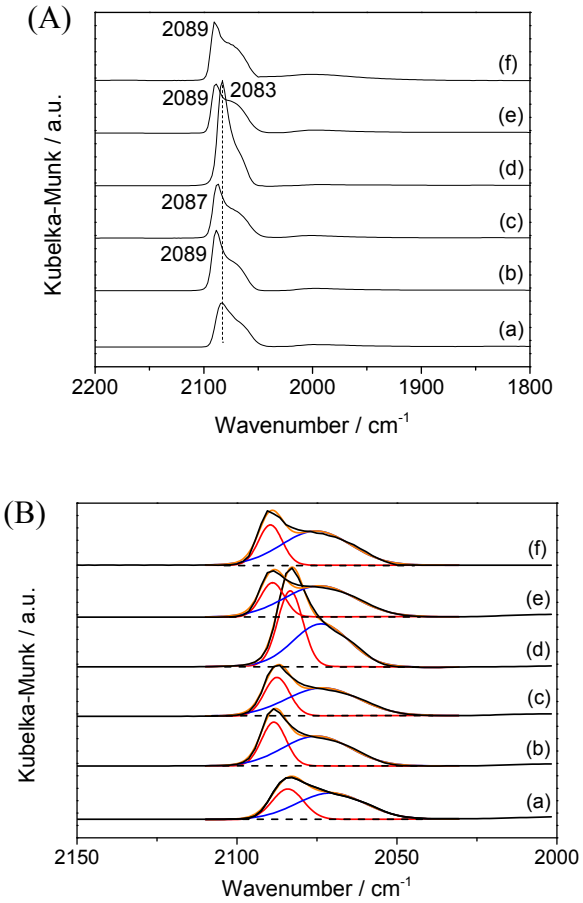

Figure 6. DRIFT spectra of CO adsorbed on the Ir-ReO_x/Rutile catalysts after reduction at 573 K. (A) The raw profiles of spectra, (B) Curve fitting results of spectra (A) at range of 2030-2110 cm^{-1} by Gaussian function and analysis results are shown in Table S7. Y-axis is normalized by corresponding D_{CO}.

(a) 4 wt% Ir/Rutile, (b) 4 wt%-Ir Ir-ReO_x/Rutile (Re/Ir = 0.24*), (c) 4 wt%-Ir Ir-ReO_x/Rutile (Re/Ir = 0.30*), (d) 2 wt%-Ir Ir-ReO_x/Rutile (Re/Ir = 0.32*), (e) 6 wt%-Ir Ir-ReO_x/Rutile (Re/Ir = 0.18*), (f) 8 wt%-Ir Ir-ReO_x/Rutile (Re/Ir = 0.15*).

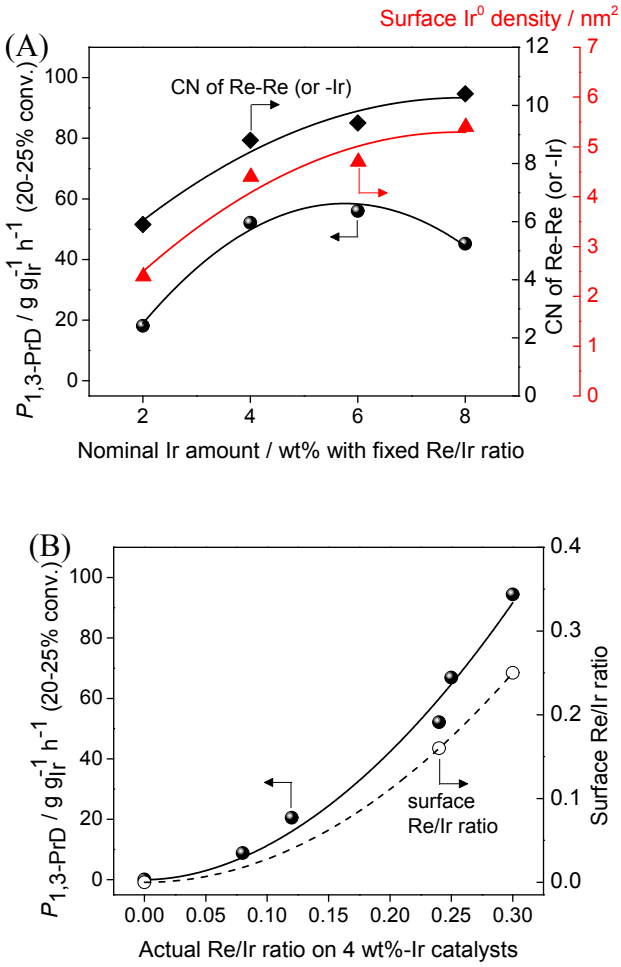

Figure 7. Relationship between catalytic performance and (A) average CN of Re-Re (or -Ir) (black curve) and the density of surface Ir^0 surface on Ir-ReO_x/Rutile catalysts with different Ir loading amount (red curve), and (B) surface Re/Ir ratio (Table 7) on 4 wt%-Ir Ir-ReO_x/Rutile catalysts. Reaction conditions: Detailed results are shown in Table S8.

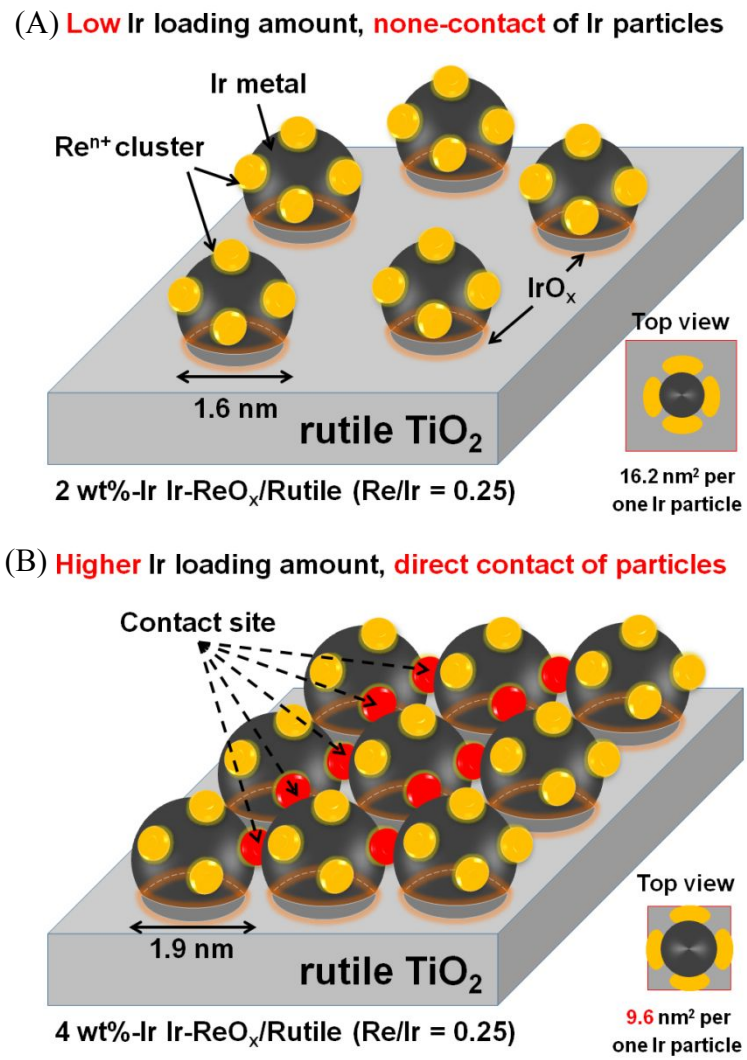

Figure 8. Proposed catalyst structure of Ir-ReO$_x$/Rutile catalyst after reduction at 573 K.

Graphic abstract

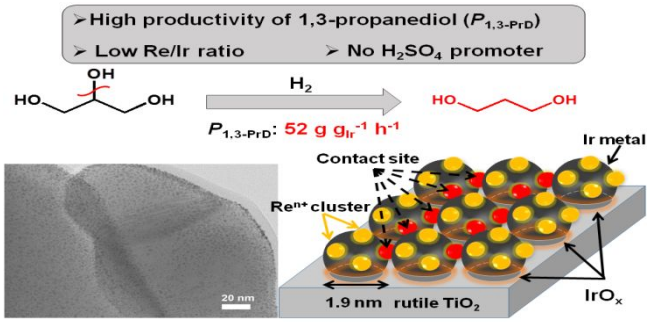

4 wt%-Ir Ir-ReO_x/Rutile (Re/Ir = 0.25) catalyst